Université de Sherbrooke
Faculté de génie
Département de génie chimique et de génie biotechnologique

Estimation de paramètres et modélisation de piles au lithium et aux ions lithium

Parameter estimation and modeling of lithium and lithium-ion batteries

Thèse de doctorat
Spécialité : génie chimique

Barzin Rajabloo

Jury : Marin Désilets (directeur)
Pierre Proulx
Marcel Lacoix
Daniel Bélanger

Sherbrooke (Québec) Canada May 2017

To my parents

To my wife and sister, Mahsa and Noushin

Résumé

Les batteries au Li-ion (BLI) figurent parmi les technologies les plus prometteuses pour le design de systèmes de stockage d'énergie à cause de leurs caractéristiques intrinsèques. Leur grand voltage de travail, leur grande densité énergétique et leur impact écologique positif expliquent l'intérêt soutenu de l'utilisation des BLI pour remplacer par exemple les moteurs à explosion dans les applications de transport terrestre. Il n'est donc pas surprenant de constater que ces technologies ont eu une attention scientifique importante et que plusieurs auteurs ont développé des modèles numériques simulant leur comportement. Il reste cependant difficile de représenter tous les phénomènes multiphysiques qui se déroulent à l'intérieur des batteries rechargeables par des modèles mathématiques. Des compromis importants doivent être faits lorsqu'on doit choisir un modèle représentant les principaux phénomènes physico-chimiques tout en restant assez simple pour pouvoir l'utiliser dans des études s'échelonnant sur de larges périodes temps. Représentant à la fois la cinétique électrochimique et le transport de masse, les modèles électrochimiques ont été introduits pour prendre en compte les phénomènes les plus importants. Ces modèles demandent cependant de connaître tous les paramètres électrochimiques, des données qui sont difficiles à obtenir expérimentalement. Les techniques d'estimation de paramètres simplifient l'obtention de ces données critiques pour représenter le comportement de la pile. Dans cette étude, une méthode d'estimation de paramètres a été introduite pour estimer les paramètres électrochimiques des BLI les plus influents, en prenant en compte différents matériaux d'électrode positive. La méthode proposée repose sur une amélioration du modèle à particule unique, qui représente lui-même une simplification du modèle pseudo-2D, le modèle électrochimique le plus connu et le plus complexe dans le domaine de la simulation de piles à électrodes poreuses. Les paramètres électrochimiques les plus importants ont été identifiés en négligeant la micro-structure de la batterie au Li-ion. Une étude de sensibilité a ensuite permis d'identifier les domaines temporels et les courants de décharge les plus favorables pour l'identification de chaque paramètre. Étant donné que le comportement des BLI dépend fortement des matériaux actifs utilisés pour la fabrication des électrodes, la méthodologie proposée a été testée sur 3 matériaux actifs différents ($LiCoO_2$, $LiMn_2O_4$ and LiFePO4) employés dans la fabrication industrielle d'électrodes positives. Finalement, une autre amélioration du modèle à particule unique a été proposée et testée afin de mieux représenter le comportement spécifique du $LiFePO_4$ (LFP), un matériau actif parmi les plus prometteurs pour l'électrode positive. Plus précisément, un modèle électrochimique simplifié incluant une équation représentant la variation de résistance en fonction du degré de décharge a été développé et les coefficients de cette équation ont été déterminés au moyen de la méthode d'estimation de paramètres proposée.

Mots-clés: Batteries au Li-ion, cellule Li/LFP, estimation de paramètres, modèle à particule unique

Abstract

Specific characteristics of Li-ion batteries (LIBs) make them promising candidates for energy storage systems when compared with the others. High working voltage and energy density as well as green technology of LIBs are the reasons for increasing interest to use these electrochemical systems as the substitute of conventional combustion engine of automobiles. Consequently, the interest to study these technologies has increased recently and several models have been introduced to simulate their behavior. However, it is difficult to model all multiphysics phenomena happening inside such rechargeable batteries. Some important choices need to be made when one wants to select an appropriate model for considering the main physics elements and yet be simple enough for large time scale studies. Combining chemical/electrochemical kinetics and transport phenomena, electrochemical models have been introduced to tackle most important principles inside the cell. These models, however, require known electrochemical parameters which most of the time are hard to get experimentally. Parameter estimation (PE) techniques simplify extracting these representative parameters of the cell behaviour. In this study, a PE methodology has been introduced to estimate the most influential electrochemical parameters of LIBs considering different positive electrode materials. The methodology starts with simplifying the well-known pseudo-two-dimensional (P2D) model, the most complex and the most popular electrochemical engineering models for simulating porous electrodes and introducing an enhanced single particle model (SPM). Neglecting the micro-structure of LIB, major electrochemical parameters are detected at the cell level. Next, the best time domains and discharge current rates to estimate each parameter are estimated by virtue of sensitivity analyses. Owing to the fact that the behavior of LIBs depends on the active materials employed in the electrode, the proposed methodology is verified for three different positive electrode active materials including $LiCoO_2$, $LiMn_2O_4$ and $LiFePO_4$. Furthermore, focusing on $LiFePO_4$ (LFP), as the most promising positive electrode active material, a new modification is proposed to the model to address special features of this material. In this regard, a simplified electrochemical model is equipped with a variable resistance equation whose coefficients are estimated by means of PE.

Key word: Li-ion batteries, Li/LFP cell, parameter estimation, single particle model

Acknowledgments

Foremost, I would like to express my sincere gratitude to my advisor Prof. Martin Désilets for his helpful advices, motivation, and continuous support. I will remember all the moments he was encouraging me during the hard times when I had lost my motivation.

My sincere thanks also goes to my thesis committee: Prof. Daniel Bélanger, Prof. Pierre Proulx and Prof. Marcel Lacroix, for their helpful comments and encouragement.

I am highly indebted to Prof. Gessie Brisard, Yves Choquette and Prof. Gaétan Lantagne, for their guidance and for providing valuable information regarding this research.

I express my special thanks and love to my friends, Mohsen Ariana, Mohammad Gholami and Ali Jokar and all other friends who have helped me during these years.

Last but not the least; I would like to thank my family: my parents, my wife and my sister for supporting me. There is no way to thank you enough. I will be always grateful to you for everything you have done for me.

Table of Contents

List of figures

List of tables

List of symbols

a_i	Specific surface of electrode i $(i = p, n)$, $\mathrm{m^2/m^3}$
c	Electrolyte concentration, $\mathrm{mol/m^3}$
$c_{s,i}$	Concentration of lithium ions in the particle of electrode i $(i = p, n)$, $\mathrm{mol/m^3}$
$c_{s,i,0}$	Initial concentration of lithium ions in the particle of electrode i $(i = p, n)$, $\mathrm{mol/m^3}$
$c_{s,imax}$	Maximum concentration of lithium ions in the particle of electrode i $(i = p, n)$, $\mathrm{mol/m^3}$
D	Electrolyte diffusion coefficient, $\mathrm{m^2/s}$
$D_{s,i}$	Lithium ion diffusion coefficient in the particle of electrode i $(i = p, n)$, $\mathrm{m^2/s}$
F	Faraday's constant, $\mathrm{C/mol}$
I	Superficial current density, $\mathrm{A/cm^2}$
i_0	Exchange current density, $\mathrm{A/cm^2}$
i_n	Transfer current normal to the surface of the active material, $\mathrm{A/m^2}$
j_i	Wall flux of Li^+ on the particle of electrode i $(i = p, n)$, $\mathrm{mol/m^2 s}$
n	Negative electrode
p	Positive electrode
r	Radial coordinate, m
R	Universal gas constant , $\mathrm{J/(mol\ K)}$
R_i	Radius of the particle of electrode i $(i = p, n)$, m
s	Separator
s	Stoichiometric coefficient, positive for anodic reactants
t_+^0	Li^+ transference number with respect to the velocity of solvent
T	Absolute temperature, K
U_i	Open-circuit potential of electrode i $(i = p, n)$, V
x	Spatial coordinate, m
x_{i0}	Initial state of charge at the electrode i $(i = p, n)$

Greek

α_i	Transfer coefficient $(i = a: \mathrm{anodic}, i = c: \mathrm{cathodic})$

ε_i	Porosity of region i $(i = p, s, n)$
τ	Tortuosity
φ_1	Solid-phase potential, V
φ_2	Solution-phase potential, V

List of abbreviations

BDS	Battery Design Studio
BMS	Battery Management System
DOD	Depth-Of-Discharge
EC	Ethylene Carbonate
ECM	Equivalent Circuit Model
EIS	Electrochemical Impedance Spectroscopy
EOCV	End Of Charge Voltage
EV	Electric Vehicle
HEV	Hybrid Electric Vehicle
HPPC	Hybrid Pulse Power Characterization
LIB	Lithium Ion Battery
MCMB	Mesocarbon microbeads
P2D	Pseudo 2 Dimensional
POD	Proper Orthogonal Decomposition
PSS	Pseudo Steady State
SEI	Solid Electrolyte Interface
SOC	State-Of-Charge
SOH	State-Of-Health
SPM	Single Particle Model

1. Introduction

1.1 Lithium ion batteries

Lithium ion batteries (LIBs) have become one of the most appropriate candidates for energy storage because of their specific characteristics in comparison with alternative technologies. In fact, their prime position in the Ragone plot (Figure 1.1) and other features including long service life, high energy-to-weight ratios, no memory effect and low self-discharge are the reasons for their success.

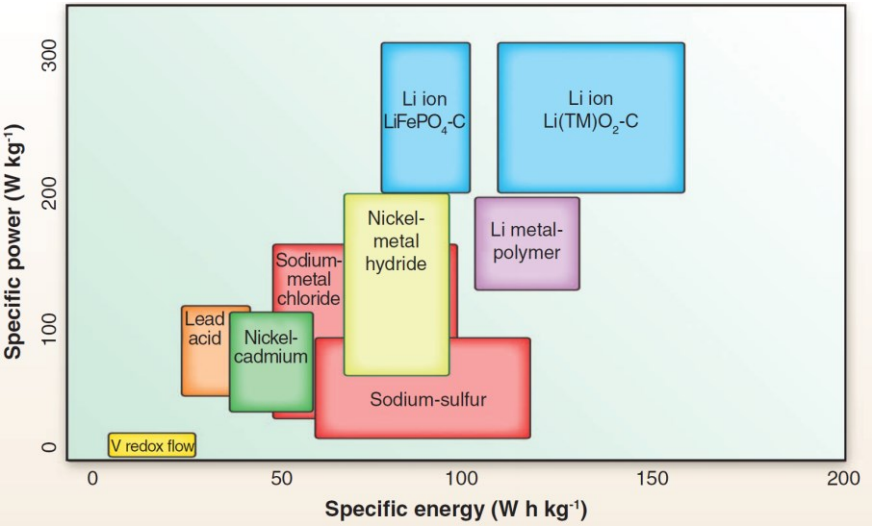

Figure 1.1: Ragone plot for different secondary batteries [1]

Figure 1.2 illustrates different types of LIBs according to cell shape and component materials. A battery consists of five regions: positive electrode, negative electrode, a separator that prevents electron to flow directly between the electrodes and two current collectors on the outside of each electrode. Usually, lithium ion batteries use a transition metal oxide as a positive electrode, carbon as the negative electrode, and a lithium salt dissolved in a nonaqueous organic solvent as the electrolyte.

During discharge, the lithium ions are shuttled from the negative electrode (anode) to the positive electrode (cathode) whereas the reverse process occurs during charge (Figure 1.3). During the discharging process, the anode undergoes an oxidation reaction and lithium ions leave the negative electrode (e.g. carbon) towards positive electrode (e.g. LFP) while electrons move in the same direction in the external circuit. Meanwhile, a reduction reaction happens at the cathode when the lithium ions and electrons combine. The reverse process takes place during the charging process.

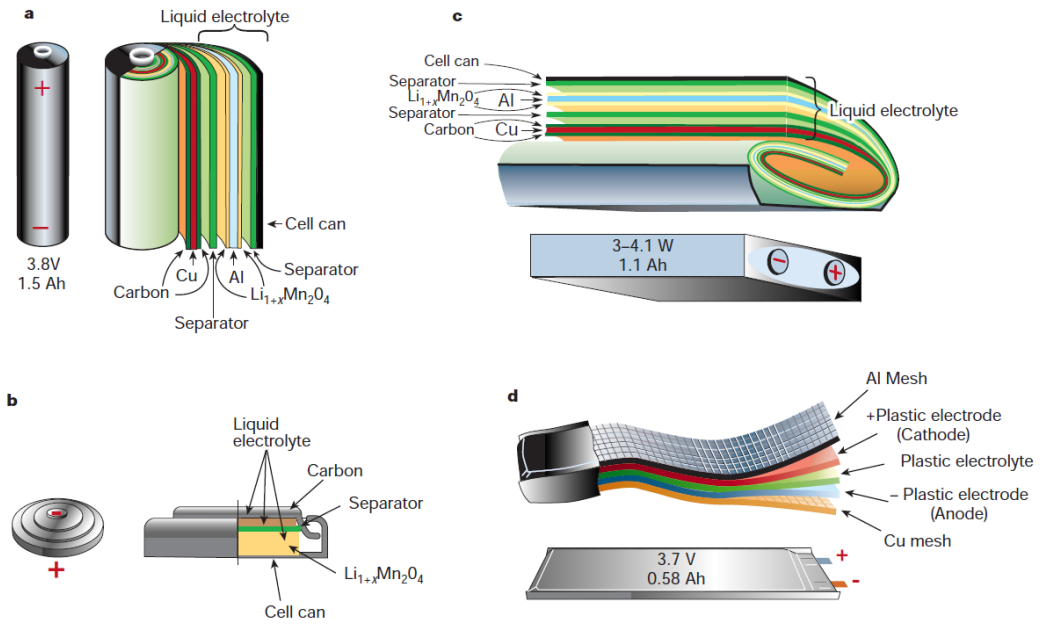

Figure 1.2: Different types of lithium secondary batteries based on their shape: (a) cylindrical, (b) coin, (c) prismatic and (d) pouch [2]

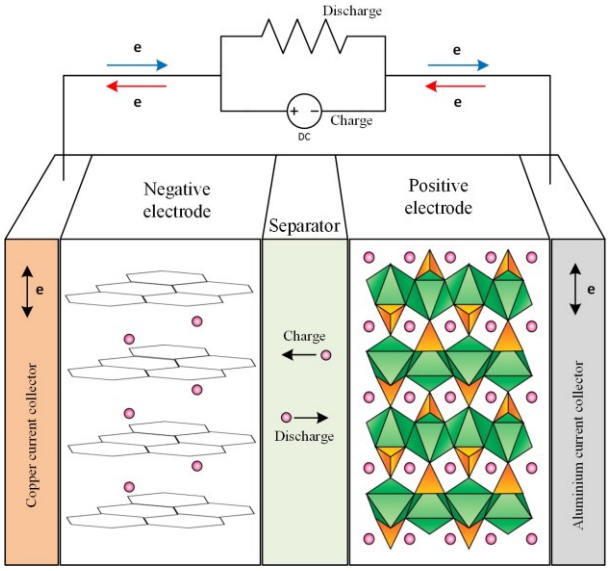

Figure 1.3: Movement of Li+ in an electrolyte and insertion/extraction of Li+ within electrodes in a lithium ion battery

The following characteristics are vital for different parts of a secondary battery. For anode materials, the potential of the electrochemical reaction should be close to the reduction potential of lithium metal. This characteristic makes it possible to provide continuous redox reactions and to maximize the performance of the cell by increasing cell voltage. Carbon-based materials are good candidates to obtain continuous, repeated redox reactions due to their stable structure. The

electrolyte should have an electrochemical and thermal stability within the range of the working conditions. For example, the temperature inside which the liquid electrolyte should be stable ranges from -20 to 60℃. Polymer electrolyte, on the other hand, is needed to be stable until 4.5 V because the typical metal oxide positive electrodes of Li-ion batteries such as $LiCoO_2$, $LiNiO_2$, and $LiMn_2O_4$ have a voltage of 4.3V in fully charged state [3]. The separator, which prevents short circuit caused by the electrical contact between the cathode and the anode, should keep its integrity at high temperatures. Stable transition metal oxides are typically used as positive electrodes to minimize the expansion/contraction caused by intercalation /deintercalation of lithium ions within lattice structure. Common cathode materials are lithium transition metal oxides such as layered $LiMO_2$ (M=Ni, Co, Mn) and spinel LiM_2O_4 (M=Ti, V, Mn) and lithium transition metal phosphates such as olivine $LiMPO_4$ (M=Fe, Co, Ni, Mn).

Among various olivine composites, $LiFePO_4$ (LFP) has found to be the most promising because of its structural and chemical stabilities. However, this active material suffers from poor electronic conductivity and low apparent lithium diffusivity. Another specific behavior of the LFP active material is a two-phase process of intercalation/deintercalation. The special treatments to overcome LFP deficiencies and its complex two-phase intercalation/ deintercalation process make it difficult to simulate this challenging technology.

1.2 BMS

To meet the power and the energy required for various applications, especially in electrical vehicle (EV), large numbers of LIBs are usually used in series and/or in parallel configurations. Monitoring the operation and controlling the working conditions of such a pack of batteries is vital. A Battery Management System (BMS) is responsible to receive input data such as the surface temperature and terminal potential from the battery pack, and to simulate the electrical behaviour of the batteries by virtue of a mathematical model (Figure 1.4). This intelligent system provides valuable information such as the State of Charge (SOC) and State of Health (SOH) of the battery pack. In addition, an active BMS can change the working conditions of batteries to optimize their lifespan and performance.

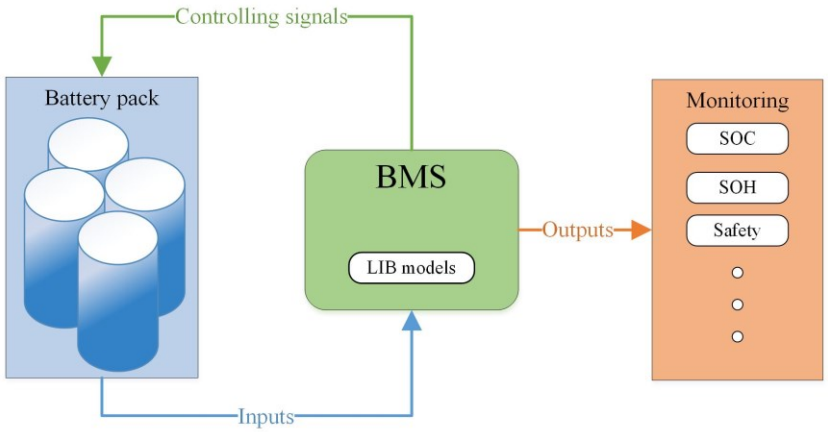

Figure 1.4: Schematic of BMS

LIB models, at the heart of BMS, can be divided into two general types: empirical-based models and electrochemical-based models. The former, which are usually used in automotive industries, are simple and fast. In fact, empirical-based models typically use previous responses of the batteries to predict the most probable future behaviors of these energy storage devices. Although they deliver a fast response, they are not able to simulate the performance of cells in working conditions that are different from the conditions used for calibrating the models.

Electrochemical-based models, on the other hand, are capable to simulate the behavior of the batteries in a wide range of operating conditions and applications. These models take into account the chemical/electrochemical kinetics and transport equations to simulate all physical phenomena happening inside the cells. Electrochemical-based models, however, are more complex and they need larger number of parameters including physical and chemical parameters. Some parameters, such as the physical dimensions and the chemistry of materials are obtainable from experimental measurements. However, some other parameters including design parameters, electrode specific parameters, kinetic parameters, etc. are hardly accessible from measurements. Parameter Estimation (PE) techniques are introduced to get around these difficulties. These techniques can also be implemented to study several dimensions of LIB performance, such as their thermal behavior and lifespan predictions.

1.3 Parameter estimation

Inverse methods are developed to estimate the unknown parameters of a system based on its measured behaviour. The idea is to minimize the difference between the experimental data reflecting the performance of the system and the simulated results. This optimization is conducted by changing the parameters systematically and iteratively (Figure 1.5). When this difference (objective function) is less than an a priori established criterion, the estimated parameters are assumed to be representative of the real physical parameters. To verify the

results, the estimated parameters should be examined in conditions beyond the ones used for PE process.

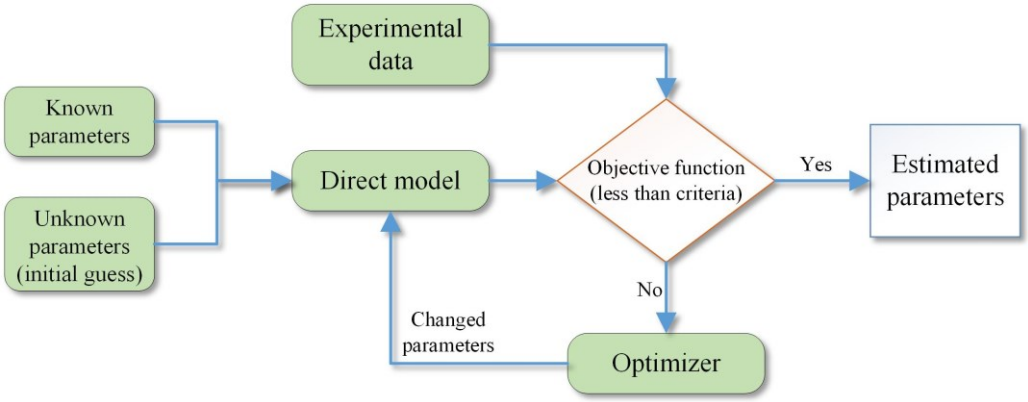

Figure 1.5: Parameter estimation process

Parameter estimation, as one of the most important deliverables of an inverse problem, depends on several factors. Initial guesses and boundaries for the estimated parameters play a vital role in PE. In addition, a well-suited direct model significantly alters the PE process. This model should be fast and simple enough to be efficiently used inside an iterative loop. At the same time, it should be accurate enough to consider important physical phenomena inside the cells. PE process also relies on the optimization process. Choosing an appropriate solution method can help to guaranty the reliability of the parameters obtained from this process.

1.4 Research project description

Generally speaking, the study of the behavior of LIBs demands to understand and implement all dominant physical phenomena happening inside the cell by virtue of a well suited electrochemical model. The governing equations to be included in such a comprehensive model need to rely on some significant parameters. These parameters, which are not facile to extract from experiment, can be estimated by PE.

Beside common major parameters found in all electrode active materials, the special features of LFP like resistive-reactant characteristics of these favorable positive electrode active materials, add more complexities to the electrochemical model. Complex models are typically not well suited for time consuming study such as predicting the life of the cell. On the other side, the importance to estimate cell parameters with a high reliability, which calls for the effectiveness of the PE procedure, and the urge to introduce a convenient model for LFP material lead us to define the basic question of the research project: ‘Can we develop a simple electrochemical model that represents the behavior of LFP positive electrode in Li-ion batteries and use it inside an inverse method in order to estimate the most influential parameters?’

The focus of this study will be on the electrochemical models introduced to simulate LIB at the cell level. In other words, the micro-structure of LIB and physical phenomena taking place in a very small time and length scale are ignored. Working on the most general yet accurate electrochemical model, PE methodology developed in this study is a good seeding point for future studies at large time and length scale such as predicting the life of LIBs or performance of LIBs in pack configuration.

1.5 Research project objectives

1.5.1 Principal objectives

The principal objectives of this study are: 1. developing a PE methodology which works for different chemistries of electrode materials used in representative working conditions, 2. introducing a simple still precise model for LFP active material using PE methodology developed as the first objective to identify the hard to get parameters.

This study will take into account the modifications of an applicable electrochemical model and using a proper optimizer.

1.5.2 Specific objectives

In order to fulfill the principal goals, other objectives should be accomplished:

1. Find and adapt a befitting direct model which includes the most important phenomena occurring inside the cell. This model needs to be as simple as possible to guaranty the convergence of the time consuming PE process.

2. Perform sensitivity analyses to detect the important electrochemical parameters and the way they influence the performance of the cell.

3. Choose an appropriate optimizer and develop a well-designed and efficient PE procedure.

4. Modify the electrochemical model to represent the special features of LFP active material while avoiding complex models. It is necessary to consider the special features of LFP through simple equations whose constants can be obtained by PE.

1.6 Contribution, originality of this study

As discussed earlier, the simulation of LIBs is of a great importance due to the increasing demand related to these technologies, especially in the automotive industries. Although

numerous researches are focusing in this field, a better understanding of this device is still of great scientific value. Moreover, varieties of electrode materials and their peculiar features call for developing specialized models. It is worth noting that the need to use more accurate and complex models than empirical relations entrains the need to find a systematic way to extract the required parameters.

The contribution and the originality of this study comprise two different aspects of the research question. In PE methodology, a systematic inverse method is applied to decipher all main electrochemical parameters. These parameters are estimated from the domains where they have higher influence on the simulated results. Incorporating a mathematical sensitivity analysis in PE procedure for the first time has strengthen the effectiveness of the procedure and the reliability of the obtained parameters. This unique methodology can be applied for any electrode active materials to efficiently estimate inaccessible parameters of the cells. The original PE process developed in this study has been verified for three different positive electrode chemistries.

For the second part of the research question, a new modification has been proposed to one of the prevalent electrochemical model in order to consider the special features of LFP as the positive electrode material. In this regard, an equation representing a variable resistance of LFP has been proposed and its coefficients have been estimated by virtue of the PE. This unique and efficient model can be incorporated into larger numerical studies without compromising accuracy and reliability.

1.7 Thesis plan

The thesis contains five chapters as follow:

State of art, as the second chapter, reviews other related studies. Besides, more detailed explanations about different LIB models have been included in this chapter. The selection of a proper electrochemical model is demonstrated. Simplifications of complex models to build a quick, simpler but accurate one are also illustrated. The PE methodology, as the first part of research question, is clarified here. Finally, to understand the importance and the influences of the main parameters on the simulation results, a sensitivity analysis is introduced and conducted in this chapter three.

The third chapter presents the implementations of the PE methodology explained in the second chapter. The methodology for estimating the needed electrochemical parameters is verified for three different positive electrode active materials including $LiCoO_2$, $LiMn_2O_4$ and $LiFeO_4$. Promising results are compared with experimental data.

In chapter 4, an electrochemical model is modified to consider the peculiar specifications of LFP as positive electrode active material. In fact, a variable resistance equation is coupled with the electrochemical kinetics and transport equations. This resistance is representing two phenomena observed at the end of the discharge process of LIBs using LFP as the positive active material including: 1. higher diffusion overpotential as Li^+ ions are intercalated inside larger particles, 2. higher ohmic resistance based on resistive-reactant feature of LFP material. The proposed model is verified for two different Li/LFP cells, designed respectively for high-energy and high-power applications. The simplicity of the model allows one to use it as an alternative of complex and time consuming models especially in large time and length scales studies.

The final chapter summarizes the conclusions of this research project. In addition, the perspectives of the project are described and subsequent objectives are briefly proposed for future works.

2. State of the art

There have been many studies on LIBs to analyze various problems such as underutilization, capacity fade, lower energy density, thermal runaway, etc. To address these issues, various experimental and computational studies have been done in different time and length scales. The first part of following section focuses on models introduced to simulate the performance of LIBs. Pseudo-two-dimensional (P2D) model and single particle model (SPM) are explained as they are the most popular electrochemical models. The second part of this chapter reviews PE studies. The methodology of PE used in this project is finally presented.

2.1 Lithium-ion batteries modeling

There are different categories for LIB modeling including empirical models, electrochemical engineering models, multiphysics models, and molecular/atomistic models.

Empirical models [4, 5] apply various functions such as polynomial, exponential, power law, logarithmic, etc. to fit experimental data. Ignoring physicochemical principles, empirical models provide fast responses and predict the future behavior of lithium-ion batteries based on historical data. Although they are easy to implement, they only work inside a specific set of operating conditions. Therefore, their predictions can be very poor when estimating other battery operating conditions.

Electrochemical engineering models provide, on the other hand, predictions that are more precise at the cost of higher complexity and longer computation time. These models incorporate chemical/electrochemical kinetics and transport phenomena and their predictions are valid inside a wide range of operating conditions. They are divided into different sub-models such as single particle models (SPM), ohmic-porous electrode models and pseudo-two-dimensional models (P2D).

Developed by Atlung *et al*. [6] and later expanded by Haran *et al*. [7], SPM is the most simplified electrochemical engineering model. It ignores the local concentration and potential in the solution phase. More precisely, the most important assumption in the SPM is about the uniform current distribution along the thickness of the porous electrodes, which results to treat the porous electrodes as a large number of single particles, all of which are subjected to the same conditions. SPMs are applicable for low applied current densities, thin electrodes, and highly conductive electrodes [8], where the overpotential is only affected by the diffusion [9, 10].

Ohmic porous-electrode models, which are more complex that SPM, consider the potential in both solid and electrolyte phases. Additional phenomena can be addressed by virtue of these

models, such as considering the conductivities as a function of the porosity [11]. Such a model has been used to design the separator and electrode thicknesses [12-14]. However, these models neglect the spatial variation in the concentration of Li^+; a similar assumption is done in SPMs.

As the most comprehensive electrochemical model, pseudo-two-dimensional (P2D) models are developed based on the concentrated solution theory. When compared to ohmic porous-electrode models, predictability was improved in P2D models by considering the diffusion in electrolyte and solid phases as well as a Butler-Volmer kinetics at both electrodes. P2D models solve the electrolyte concentration, electrolyte potential, solid-state potential, and solid-state concentration within the porous electrodes. It also solves the electrolyte concentration and potential within the separator. Similar models have been developed based on the P2D model [10, 15-22].

Combining the electrochemical behavior of batteries with other aspects of these systems such as thermal and mechanical features leads to another category of LIB modeling, called multiphysics models. Among different multiphysics models, thermal modeling includes Joule heating effects into one of the electrochemical engineering models while the stress-strain models consider expansion and contraction due to the intercalation/deintercalation of lithium into/from the electrode active material.

At smaller time and length scales, the molecular/atomic models are introduced using a stochastic approach to simulate the diffusion of lithium from site to site within an active particle [23-25].

2.1.1 Pseudo-two-dimensional (P2D) model

The equations required to simulate the electrochemical performance of porous electrodes with concentrated electrolytes are based on the porous electrode and concentrated solution theories. The basis of these theories has been reviewed by Newman and Tiedemann [26]. In the porous electrode theory, instead of taking into account the exact position and shapes of all particles and pores, properties are averaged over a control volume big enough with respect to the pores so as to use continuity equations, but small enough with respect to the overall volume of the electrode.

The electrode is treated as a superposition of active material, filler, and electrolyte, and these phases coexist at every point in the model, each of with known volume fraction. Without considering the detailed pore geometry, the porous electrode is described by specific (interfacial) area, a, and volume fraction of each phase ε. The electrochemical reaction at the surface becomes a homogeneous reaction because of the existence of the interface between the two phases at each point in the volume of the electrode.

The effective parameters, such as the effective diffusivity of electrolyte in this porous structure, D_{eff}, can be calculated by

$$D_{eff} = D\left(\varepsilon/\tau\right) \tag{2.1}$$

Where D is the intrinsic diffusivity (bulk value) of the Li ions in the electrolyte, ε is volume fraction of the porous structure and τ is the tortuosity of active material , which is usually related to the porosity by the Bruggeman relation [27].

$$\tau = \varepsilon^{-0.5} \tag{2.2}$$

Generally, the particles of the active material can be treated as spheres. The interfacial area (a) is equal to the surface area of each sphere times the number of spheres per unit volume (N_p):

$$a = N_p\left(4\pi R^2\right) \tag{2.3}$$

The volume fraction occupied by the solid material (ε_s) is equal to the volume per sphere times the number of spheres per unit volume:

$$\varepsilon = N_p\left(4/3\pi R^3\right) \tag{2.4}$$

Eliminating N_p, the interfacial area can be solved from known quantities like volume fraction of solid material and particle radius:

$$a_i = 3\varepsilon_i / R_i \tag{2.5}$$

Where $i = p\ , n$ as positive and negative electrode respectively.

P2D model consists of a set of six equations, to be solved for the following variables [28]:

- ϕ_1 Solid Phase Potential
- ϕ_2 Solution Potential
- c Lithium ion concentration in the solution
- c_s Lithium concentration in the electrode at the electrode/electrolyte interface
- i_n Reaction rate
- i_2 Solution phase current density

As mentioned earlier, the focus of this project is on SPM, inside which the potential and concentration of Li^+ in the solution are assumed as constants. Therefore, only two variables, the reaction rate and concentration of ions inside the solid phase, and the corresponding equations that need to be solved in the SPM, will be explained here.

2.1.1.1 Reaction rate

The dependency of the local electrochemical reaction rate on the concentration and potential is usually determined by the Butler-Volmer rate equation:

$$i_n = i_0\left[exp\left(\frac{\alpha_a F\left(\phi_1-\phi_2-U\right)}{RT}\right)-exp\left(\frac{-\alpha_c F\left(\phi_1-\phi_2-U\right)}{RT}\right)\right] \tag{2.6}$$

The surface overpotential, $\phi_1-\phi_2-U$, is the deviation from the thermodynamic potential difference between the solid and the solution at the existing surface concentrations. U is the open-circuit potential of the solid material evaluated at the surface concentration (a function of intercalant concentration). The α_a, α_c are the anodic and cathodic transfer coefficients, respectively. The exchange current density, i_0, is the reference current for the system based on kinetics of the reaction. It is a function of the lithium concentrations in electrolyte and solid active materials, i.e:

$$i_0 = F\left(K_a\right)^{\alpha_c}\left(K_c\right)^{\alpha_a}\left(c\right)^{\alpha_a}\left(c_{s,max}-c_{s,e}\right)^{\alpha_a}\left(c_{s,e}\right)^{\alpha_a} \tag{2.7}$$

Where c and c_s are the volume-averaged lithium concentration in the electrolyte and solid phases, respectively, $c_{s,e}$ is the area-averaged solid-state lithium concentration at the electrode/electrolyte interface, and $c_{s,max}$ is the maximum concentration of lithium in the solid phase. K_a and K_c are the rate constants for the anodic and cathodic directions of a reaction, respectively.

2.1.1.2 Transport in the solid

The porous electrode is approximated as a collection of evenly sized spheres. Neglecting the effects of stress, anisotropic diffusion and volume changes in the solid and assuming a good electrical conductivity of active material as well, the transport of lithium ions can be described by the Fick's law in spherical coordinates:

$$\frac{\partial c_s}{\partial t} = \frac{1}{r^2}\frac{\partial}{\partial r}\left(D_s r^2 \frac{\partial c_s}{\partial r}\right) \tag{2.8}$$

With the boundary conditions:

$$\left.\frac{\partial c_s}{\partial r}\right|_{r=0} = 0 \quad and \quad -D\left.\frac{\partial c_s}{\partial r}\right|_{r=R} = j_{Li^+} \tag{2.9}$$

And with the following initial condition:

$$c_s\left(t=0,r\right) = c_s^0 \tag{2.10}$$

Where j_{Li^+} is the flux of lithium at the particle surface due to the electrochemical reaction and D_s is the diffusion coefficient. The boundary condition at the interface of solid particles and electrolyte is responsible for the coupling between the electrochemical reaction rate and the mass balance in the solid.

2.1.2 Single particle model (SPM)

Aiming to simplify the P2D model, the single particle model (SPM) has been introduced based on two main assumptions: First, a uniform current distribution is assumed along the thickness of the porous electrode. Second, the electrolyte potential and concentration are supposed to be constant. These assumptions allow representing the entire porous electrode by a single intercalation particle [8]. Figure 2.1 demonstrates SPM for the discharge process schematically.

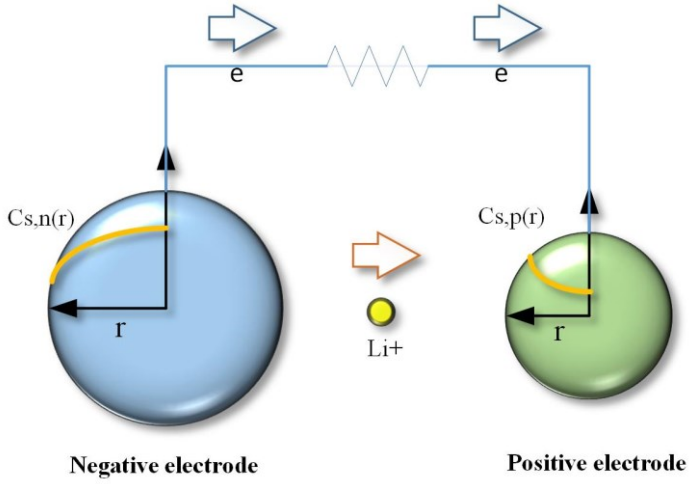

Figure 2.1: SPM for discharge process

In SPM, the material balance for the lithium ions inside the electrode active material can be represented by the Fick's law in spherical coordinates (Eq. 2.8). Like in P2D model, the Butler-Volmer kinetics equation (Eq. 2.6) is also representing the reaction rate.

The molar flux of lithium ions in SPM is related to the total current *I* passing through the cell:

$$J_j = \frac{I}{FS_j} \tag{2.11}$$

Where F is Faraday's constant and S_j is the total electroactive surface area of electrode j

$$S_j = \frac{3\varepsilon_j V_j}{R_j} \tag{2.12}$$

Where ε_j is the volume fraction of the solid phase active material in electrode j and V_j is the total volume of that electrode.

Simplicity and minimum computational requirements make SPM a good candidate for time-consuming studies such as life modeling [29, 30] and where a fast response is needed such as online estimation [10]. It is also more facile to implement some modifications in SPM. For example, Safari *et al*. [31] assumed four groups of particles with different connectivities to the matrix to address the resistive-reactant feature of LFP as the positive active material. Adding electrolyte concentration [32] and potential [33] inside SPM model improves the results for higher rates of charge or discharge simulations.

2.2 Parameter estimation (PE)

Electrochemical models need known parameters to simulate the behavior of the cells. The number of these parameters reflects the complexity of the model. PE is an applicable tool to find the parameters that are difficult to measure or to extract from experiments. Here, some studies using PE are summarized and the methodology for this technique is later described.

In 2007, Santhanagopalan *et al*. [34] performed a PE to estimate internal parameters of a lithium cobalt oxide/carbon (MCMB) cell. These parameters were the diffusivity of Li^+ ions in the positive electrode ($D_{s,p}$), the reaction rate constants at the electrodes/electrolyte interfaces (K_n and K_p) and the initial State Of Charge of negative and positive electrodes ($SOC_{n,0}$ and $SOC_{p,0}$). They illustrated that the SPM model they have used inside their PE is valid for low discharge

rates (<1C). However, the P2D model provides accurate results for the charge/discharge rates up to 2C at the cost of longer simulation times.

An interesting application for PE is to study the variation of influential parameters during the life of batteries. PE finds the parameters value by analyzing the experimental data after a determined period or cycle numbers in specific working conditions. Then, these parameters are introduced as functions of time or/and cycle numbers. Using an appropriate model, which is a representative of the behavior of batteries, this methodology can even help to determine and understand the origin of aging in particular conditions.

With the aim of quantifying the capacity fade of a MCMB/$LiCoO_2$ battery, Santhanagopalan *et al*. [35] estimated some significant parameters of the cell including the SOC of the negative and positive electrodes ($SOC_{n,0}$ and $SOC_{p,0}$) and the active material loading of electrodes (w_p and w_n). They studied the loss of active material and the loss of cyclable lithium under different temperature conditions.

In 2011, Ramadesigan *et al*. [36] applied a PE with a simplified P2D model to clarify the changes in significant parameters as the cell is aged. The estimated parameters in this work were the effective diffusion coefficient of lithium ion in the solution phase (D), effective diffusion coefficient of lithium in the solid phase for the negative and positive electrodes (D_{sn} and D_{sp}), and the electrochemical reaction rate constants for the negative and positive electrodes (k_n and k_p). Monotonic reduction of the effective solid-phase diffusion coefficient and of the electrochemical reaction rate constant at the negative electrode with cycle number illustrated the influence of negative electrode properties on the aging of battery. Ramadesigan *et al*. were able to extrapolate the change in those parameters with cycle number to predict the capacity fade.

In 2013, Marcicki *et al*. [37] introduced a modified SPM considering concentration and potential dynamics of the liquid phase. They estimated the electrochemical parameters and their Arrhenius temperature dependence in various steps. First, the active material volume fractions and utilization windows were estimated from OCP data. In the next step, the resistance parameters were determined, and finally diffusion parameters related to the model were extracted. They also included a time-variable resistance to capture the resistive-reactant feature of LFP positive electrode material.

Utilizing multi-objective genetic algorithm, Zhang *et al*. [38] identified the parameters of $LiCoO_2$ and $LiFePO_4$ Li-ion batteries. Considering the experimental results obtained at two temperature (15℃ and 30℃), they introduced four objective functions including terminal

voltage and surface temperature to estimate 25 parameters. A good agreement was achieved between the experimental data and the simulated results in low discharge rates.

PE studies differ in terms of the optimizers used to minimize the error between experimental data and simulated results and of the direct models implemented inside the resolution of the inverse problem. Some well-known optimizers in Li-ion battery parameterizations are Levenberg-Marquardt method [34, 35], Genetic Algorithm [38-40], Homotopy optimization method [41], and Particle Swarm optimization [42]. In regards of the direct model, most of the studies use a simplified/reduced P2D model or a modified SPM [36, 37, 41, 42]. In fact, the complexity of the resolution process and the accuracy needed for PE demand the use of a simple yet reliable model. In the first part of this study, a modified SPM was implemented to simulate the behaviour of Li ion batteries with different cathode materials. The resistivity of the electrolyte is considered by virtue of a time and current varying resistance. Moreover, as one of the most suitable optimizer, Genetic Algorithm was applied to perform PE. In the following, the important features about PE are summarized.

2.2.1 Parameter estimation process

In general, PE is an inverse problem in which the unknown parameters are estimated by means of comparisons between the experimental data and simulated results (see Figure 1.5). The difference between the experiments and predictions becomes the objective function. An optimizer is used as a mathematical tool to minimize the objective function and to compute the vector of parameters, which are the output of a PE study.

The experimental data in Li-ion battery parameterization is most of the time the values of the terminal voltage extracted from charge/discharge process in N time intervals from zero to cutoff time (t_c) as shown in Eq. (2.13)

$$\mathbf{V}_{cell}^{*} = \begin{bmatrix} V_1^{*} \\ V_2^{*} \\ \vdots \\ V_N^{*} \end{bmatrix}_{N\times 1} \qquad 0 \le t = t_1, t_2, ..., t_N \le t_c \tag{2.13}$$

Typically, the objective function (S) is defined as the ordinary least-squares function of the measured data ($\mathbf{V}_{cell}^{*}$) and the calculated values ($\mathbf{V}_{cell}$) [43]:

$$S = \left(\mathbf{V}^{*}_{cell} - \mathbf{V}_{cell}(\mathbf{P})\right)^{T} \left(\mathbf{V}^{*}_{cell} - \mathbf{V}_{cell}(\mathbf{P})\right) = \sum_{i=1}^{N} \left(V^{*}_{cell,i} - V_{cell,i}(\mathbf{P})\right)^{2} \tag{2.14}$$

The superscript T indicates the transpose. When the experimental data are collected from M charge/discharge processes, the objective function becomes:

$$S = \left(\mathbf{V}^{*}_{cell} - \mathbf{V}_{cell}(\mathbf{P})\right)^{T} \left(\mathbf{V}^{*}_{cell} - \mathbf{V}_{cell}(\mathbf{P})\right) = \sum_{m=1}^{M} \sum_{n=1}^{N} \left(V^{*}_{cell,i} - V_{cell,i}(\mathbf{P})\right)^{2} \tag{2.15}$$

The vector of parameters, **P**, is a set of required parameters such as diffusion coefficients, initial SOC, reaction rates and porosity of electrode. This vector is estimated by minimizing the objective function in the following conditions:

$$\min S = S(\mathbf{P}) \; subject\, to \, P_{j,low} \le P_{j,1} \le P_{j,high} \tag{2.16}$$

$P_{j,low}$ and $P_{j,high}$ are the minimum and maximum of the P_j values respectively.

Choosing an appropriate optimizer is important in PE studies. High number of parameters rise the risk of finding local minimum instead of determining a global one. It is worth noting that the optimizer types can be divided in two categories: 1- deterministic and 2- stochastic methods. Both categories have their positive points and drawbacks. Deterministic methods are faster than stochastic ones. However, they are more complex to implement and the risk of finding local extremum is higher in these methods. Stochastic techniques, on the other hand, are the better candidates for PE of a system with numerous unknown parameters because of their random-based operation functions [44].

To increase the speed of optimization, especially when one of the stochastic method is used, sensitivity analysis is an effective technique to be used in a preliminary step to increase the performance of the method. It helps to detect the most influential parameters and the best time domains for their estimation. Recently, Jokar *et al*. [40] performed sensitivity analyses to evaluate the parameters of a SPM representing graphite/$LiCoO_2$ Li-ion battery. Implementing a GA optimizer, they estimated 10 parameters of a simplified P2D model. The unknown parameters include the solid diffusion coefficients ($D_{s,n}$ and $D_{s,p}$), the intercalation/deintercalation reaction-rate constants (K_n and K_p), the initial SOC ($SOC_{n,0}$ and $SOC_{p,0}$), the electroactive surface areas (S_n and S_p) and two unknown variables used in the formulation of the electrolyte potential drop function. In addition, they performed six scenarios to illustrate the improvements achieved with the use of a sensitivity analysis and their special methodology. In general, the sensitivity or the Jacobian matrix (**J**) is the first order partial

derivatives of the calculated cell potential ($\mathbf{V}_{cell}(\mathbf{P})$) with the respect to the unknown parameters ($\mathbf{P}_j$):

$$\mathbf{J}\left(\mathbf{P}_j\right)=\left[\frac{\partial \mathbf{V}_{cell}^{T}}{\partial \mathbf{P}_j}\right]^{T} \tag{2.17}$$

The Jacobian value for each parameter changes with the discharge time and discharge rate. Therefore, it is possible to find the period and the rate when the voltage of the cell is more sensitive to a specific parameter.

Jokar *et al*. [40] divided the galvanostatic discharge curves of a graphite/LCO battery into three distinct regions (Figure 2.2): 1. the beginning of discharge curve; 2. the discharge cell voltage plateau; and 3. the end of discharge process.

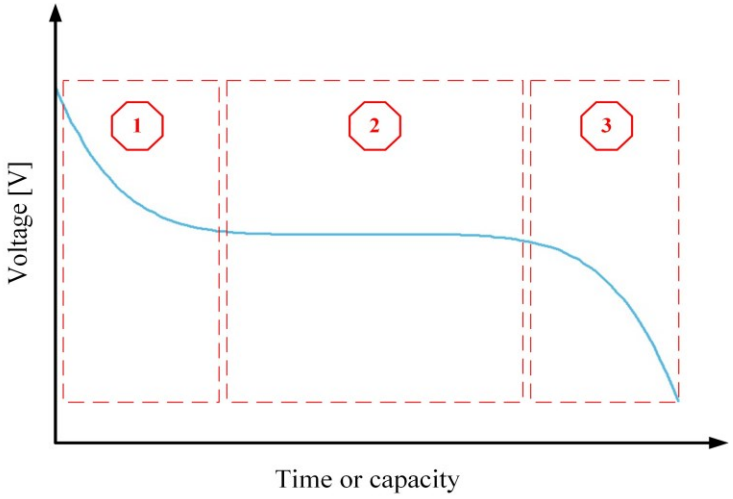

Figure 2.2: Different time domains for estimating electrochemical parameters

According to their sensitivity analysis, Jokar *et al*. [40] allocated each region to estimate particular parameters. Table 2.1 summarizes the outcomes of their study.

To validate their methodology, Jokar *et al*. [40] used reference data generated from a P2D model available in COMSOL® Multiphysics V. 5.1. To make the data even more close to reality, they also added random noises.

Table 2.1: Best time domains for PE of different electrochemical parameters of a graphite/LCO cell

Symbol	Unit	Time domain & rate
$D_{s,p}$	m^2/s	Region 2 in low and high discharge rates
$D_{s,n}$	m^2/s	Region 2 in low discharge rate – Region 3 in high discharge rate
K_p	$m^{2.5}/mol^{0.5}$ s	Region 2 in low and high discharge rates
K_n	$m^{2.5}/mol^{0.5}$ s	Region 2 in low and high discharge rates
S_p	m^2	Region 1 and 3 in all discharge rates
S_n	m^2	Region 3 in all discharge rates
$SOC_{p,0}$	-	Region 1 and 3 in all discharge rates
$SOC_{n,0}$	-	Region 3 in all discharge rates

The methodology introduced by Jokar *et al*. [40] was later verified by Rajabloo *et al*. [45] and applied to various cathode positive electrode active materials. The next chapter deals with implementation of PE process for $LiCoO_2$, $LiMn_2O_4$ and $LiFePO_4$.

CHAPITRE 3 : AVANT-PROPOS

Auteurs et affiliation:

- Barzin Rajabloo: étudiant au doctorat, Université de Sherbrooke, Faculté de génie, Département de génie chimique et de génie biotechnologique.
- Ali Jokar: étudiant au doctorat, Université de Sherbrooke, Faculté de génie, Département de génie chimique et de génie biotechnologique.
- Martin Désilets: professeur, Université de Sherbrooke, Faculté de génie, Département de génie chimique et de génie biotechnologique.
- Marcel Lacroix: professeur, Université de Sherbrooke, Faculté de génie, Département de génie mécanique.

Date d'acceptation: 10 Décembre 2016

État de l'acceptation: version finale publiée

Revue: Journal of The Electrochemical Society

Référence: [45]

Titre français: Méthode inverse pour l'estimation de paramètres électrochimiques de piles au Li-ion. Partie II : Mise en œuvre.

Contribution au document: Cet article démontre la performance d'une nouvelle méthode d'identification de paramètres de modèles électrochimiques représentant le comportement de piles au Li-ion. La méthode est appliquée avec succès à 3 types de piles différentes ce qui prouve la validité du modèle simplifié et de la méthode inverse.

Résumé français : Cet article est la deuxième partie d'une étude portant sur l'estimation de paramètres de piles au Li-ion. La méthodologie avait été développée au préalable dans la partie I. Dans la partie II, la méthodologie est testée pour trois piles utilisant des matériaux d'électrodes positives différents : $LiCoO_2$, $LiMn_2O_4$ et $LiFePO_4$. Une méthode inverse combinée à une version simplifiée du modèle P2D est utilisée pour identifier les paramètres électrochimiques suivants : Coefficients de diffusion ($D_{s,n}$ and $D_{s,p}$), constantes de réaction d'intercalation / désintercalation (K_n and K_p), état de charge initial ($SOC_{n,0}$ and $SOC_{p,0}$) et les surfaces électroactives (S_n and S_p) d'une pile au Li-ion. Les mesures expérimentales du potentiel pour

des condition de décharge lentes et rapides ont été utilisées comme données de référence au sein de la fonction objective de la méthode inverse en utilisant le meilleur intervalle de temps, celui identifié dans l'étude de sensibilité. Pour tous les cas simulés, les prédictions numériques représentent de façon fidèle les données expérimentales.

3. An inverse method for estimating the electrochemical parameters of lithium-ion batteries, Part II: Implementation

3.1 Abstract

This paper is the second part of a two part study on parameter estimation of Li-ion batteries. The methodology was developed in Part I. In Part II, the methodology is tested for $LiCoO_2$, $LiMn_2O_4$ and $LiFePO_4$ positive electrode materials. An inverse method combined to a simplified version of the Pseudo-two-Dimensional (P2D) model is used to identify the solid diffusion coefficients ($D_{s,n}$ and $D_{s,p}$), the intercalation/deintercalation reaction-rate constants (K_n and K_p), the initial SOC ($SOC_{n,0}$ and $SOC_{p,0}$), and the electroactive surface areas (S_n and S_p) of Li-ion batteries. Experimental cell potentials for both low and high discharge rates provide the reference data for minimizing the objective function in the best time interval. For all cases simulated, the numerical predictions show excellent agreement with the experimental data.

Keywords: Parameter estimation; Inverse method; Li-ion battery; Simplified P2D model; Sensitivity analysis, Genetic Algorithm (GA); LFP

3.2 Introduction

Lithium-ion (Li-ion) batteries are increasingly employed for energy storage. Their working voltage and energy density are higher than those of similar energy storage technologies. Their service life is longer. They exhibit high energy-to-weight ratios and low self-discharge. As a result, they have become the preferred energy storage devices in the electronics and the automotive industries.

Mathematical modeling of Li-ion batteries is an essential engineering tool for their design and operation. Two different approaches are usually adopted to predict their behavior. These approaches may be divided, broadly speaking, into empirical models and electrochemical models.

Empirical models are the simplest mathematical models. They are relatively easy to implement and they provide fast responses. This is why they are mostly suited for control systems used in the high tech industry and in the automotive industry. The scope of applications of empirical models is however narrow. Empirical models ignore the physical phenomena that take place in the cell. Consequently, they cannot predict the life and the capacity fading of the battery. Furthermore, they are only valid for the battery for which they have been developed [46-48].

Electrochemical models provide, on the other hand, reliable responses of the battery under a wide range of operating conditions and for different applications. They account for the chemical/electrochemical kinetics and the transport phenomena. Electrochemical models are unequivocally superior to empirical models. But they are also more complex and require longer computation times.

Among the electrochemical models, the Pseudo-two-Dimensional (P2D) model stands out. The P2D model rests on the porous electrode theory, the concentrated solution theory and the use of appropriate kinetics equations [4-6]. A simplified and computationally efficient version of the P2D model is the Single Particle Model (SPM). In the SPM, it is assumed that the current distribution along the thickness of the porous electrode remains uniform and that the electrolyte properties are constant [11, 50].

Both empirical and electrochemical models need to be calibrated in order to simulate faithfully the Li-ion cells. Moreover, due to their complexity, electrochemical models require extensive data such as the chemical/electrochemical parameters and the physical properties of the battery. Some of these parameters are readily available. They are provided by the manufacturer or can be determined experimentally. Others like the mass transport properties, the charge transfer and the kinetics parameters are more difficult to determine. This is the case of internal parameters such as the diffusivity of Li^+ ions in the electrodes ($D_{s,n}$ and $D_{s,p}$), the reaction rate constants at the electrodes/electrolyte interface (K_n and K_p), the initial State Of Charge of the electrodes ($SOC_{n,0}$ and $SOC_{p,0}$) and the volume fraction of active material in the electrodes (ε_n and ε_p), etc [34-39,42 , 51]. In this case, the collected experimental data must be processed with optimization methods in order to reveal unknown parameters and properties. A literature review of the methods applied to Li-ion batteries, i.e., the Parameter Estimation methods (PE), is provided in the first part of this study [40]. An innovative inverse PE method for identifying the electrochemical parameters of Li-ion batteries was also proposed in Part I. This inverse PE method rests on a simplified version of the P2D model combined with an inverse method and sensitivity curves of the expected parameters. The PE method may predict the solid diffusion coefficients ($D_{s,n}$ and $D_{s,p}$), the intercalation/deintercalation reaction-rate constants (K_n and K_p), the initial SOC ($SOC_{n,0}$ and $SOC_{p,0}$), and the electroactive surface areas (S_n and S_p) of the Li-ion battery. A Genetic Algorithm (GA) is used to minimize the objective function. The results displayed in Part I show good agreement between the predicted discharge curves and the noisy reference data at both low and high discharge rates.

The present paper follows Part I by verifying the proposed methodology for Li-ion cells made of different active cathode materials. The noisy reference data that were generated with the P2D model and used for validating the PE model in Part I are now substituted with actual experimental data. These data come from Li-ion batteries made of different positive electrode materials: $LiCoO_2$ (LCO), $LiMn_2O_4$ (LMO) and $LiFePO_4$ (LFP).

In the following section, the simplified P2D model, introduced in starting of paper, is reviewed. Next, the Parameter Estimation method is presented. The reference data and the expected parameters are discussed afterward. Sensitivity analysis section focuses on the sensitivity analysis of the Li-ion batteries. The features of the LFP and the challenges of simulating this positive electrode active material are discussed in Results and discussion section. Finally, the PE results are presented in Conclusion section.

3.3 Direct model

Empirical and electrochemical models are the preferred approaches for simulating the State of Charge (SOC) and the State of Health (SOH) of Li-ion batteries [11, 46, 52].

Empirical models rely on polynomial, exponential, power law, logarithmic, and trigonometric functions to match the experimental data. These models are simple and computationally inexpensive. They are however solely applicable to the battery for which they were calibrated. As a result, the scope of applications of empirical models is limited [4, 5].

Electrochemical models are, on the other hand, unquestionably superior to empirical models for predicting the behavior of Li-ion batteries. These models take into account the chemical/electrochemical kinetics and the transport phenomena that take place into the battery. But their complexity may be a drawback. They are also CPU time consuming.

The P2D model is a popular electrochemical model [6]. The P2D model considers both the diffusion and the potential in the solid and in the electrolyte phases. The kinetics is described by the Butler-Volmer expression. The P2D model solves the electrolyte concentration, the electrolyte potential, the solid-state potential, and the solid-state concentration within the porous electrodes. It also predicts the electrolyte concentration and the electrolyte potential within the separator. The transport phenomena, the electrochemistry, and the thermodynamics are portrayed by coupled nonlinear partial differential equations (PDEs) in space and time [15-21, 28, 50].

Most P2D models are, however, elaborate and CPU time consuming. A simplified version of the P2D model is the SPM, which was developed by Atlung *et al*. [6] and later improved by Haran *et al*. [7] The SPM accounts for a lumped solution resistance and it ignores the local concentration and potential in the solution phase. It also assumes that the current distribution along the thickness of the porous electrode is uniform. As a conclusion, each electrode is modeled as one spherical particle. Intercalation and de-intercalation phenomena happens through a reaction at the surface and a diffusion inside spherical particle. It should be noted that assuming uniform current distribution and ignoring concentration and potential in the solution

phase are not always possible. As a result, the SPM is most suitable for simulating Li-ion batteries with thin and highly conductive electrodes subjected to low current densities [8].

As a compromise between the simplicity of the SPM model and the accuracy of P2D models, a simplified version of the P2D model was introduced in Part I. It rests on the following equations:

$$V_{cell} \approx \left(U_p - U_n\right) + \frac{2RT}{F}\ln\left(\frac{\sqrt{m_p^2+4}+m_p}{2}\right) + \frac{2RT}{F}\ln\left(\frac{\sqrt{m_n^2+4}+m_n}{2}\right) + \frac{I}{a_0 + a_1(It) + a_2(It)^2 + \ldots} \tag{3.1}$$

where

$$m_p = \frac{I}{FK_p S_p c_{s,p}^{\max} c_e^{0.5}\left(1-SOC_p\right)^{0.5}\left(SOC_p\right)^{0.5}};\quad S_p = \frac{3\varepsilon_p V_p}{R_p},\quad SOC_p = \frac{c_{s,p}^{surf}}{c_{s,p}^{\max}} \tag{3.2}$$

$$m_n = \frac{I}{FK_n S_n c_{s,n}^{\max} c_e^{0.5}\left(1-SOC_n\right)^{0.5}\left(SOC_n\right)^{0.5}};\quad S_n = \frac{3\varepsilon_n V_n}{R_n},\quad SOC_n = \frac{c_{s,n}^{surf}}{c_{s,n}^{\max}} \tag{3.3}$$

$$SOC_k = SOC_{k,0} - \frac{J_k R_k}{c_{s,k}^{\max} D_{s,k}}\left[3\frac{D_{s,k}}{R_k^2}t + \frac{1}{5} - \sum_{k=1}^{\infty}\frac{2}{\lambda_k^2}\exp\left(-\frac{\lambda_k^2 D_{s,k}}{R_k^2}t\right)\right];\ \sin(\lambda_k) - \lambda_k\cos(\lambda_k) = 0 \tag{3.4}$$

SPM differs to simplified P2D model in last term of potential equation (Eq.1) where a lump solution resistance has been replaced by a varying resistance as a function of capacity. The derivation of the potential equation is explained in paper Part I.

The potential equation is applied in the PE process for which the electrochemical parameters and the unknown variables of the electrolyte potential drop function are estimated.

The proposed simplified P2D model improves the results of the SPM particularly at high C-rate charge/discharge. Moreover, the number of parameters needed for the simplified P2D model is less than that for the P2D model. As a result, the proposed simplified P2D model is befitting online simulation and optimization.

3.4 The parameter estimation process

Inverse problems belong to a class of ill-posed mathematical problems. Their solution is strongly dependent on the initial conditions, on the boundary conditions and on the measured signals. This makes the solution of inverse problems more challenging than that of direct problems.

In PE problems, the unknown parameters of a system can be determined with an inverse method. Of course, the parameters should be measurable and identifiable. Figure 3.1 depicts a schematic of the PE procedure [40].

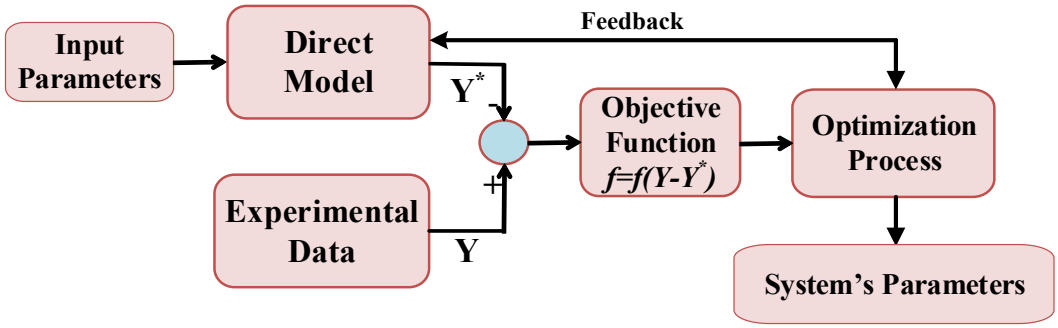

Figure 3.1: Solution procedure for inverse problems [40]

The objective function for the identification of the Li-ion parameters is defined as the difference between the experimental data for the time-varying cell potential and the numerical predictions generated by the direct model.

The vector of experimental data ($\mathbf{v}^*_{cell}$) is comprised of N time intervals between zero and the cut-off time ($0 < t \leq t_c$). It is expressed as

$$\mathbf{V}^*_{cell} = \begin{bmatrix} V^*_1 \\ V^*_2 \\ \vdots \\ V^*_N \end{bmatrix}_{N\times 1} \cdot t = t_1, t_2, \ldots, t_N \tag{3.5}$$

The objective function (S) is defined as the ordinary least-square function of the experimental data ($\mathbf{v}^*_{cell}$) and the numerical predictions ($\mathbf{v}_{cell}$) [43] for one charge or discharge cycle:

$$S = \left(\mathbf{V}^*_{cell} - \mathbf{V}_{cell}(\mathbf{P})\right)^T \left(\mathbf{V}^*_{cell} - \mathbf{V}_{cell}(\mathbf{P})\right) = \sum_{i=1}^{N} \left(V^*_{cell,i} - V_{cell,i}(\mathbf{P})\right)^2 \tag{3.6}$$

For M charge/discharge processes [34]:

$$S = \left(\mathbf{V}^{*}_{cell} - \mathbf{V}_{cell}(\mathbf{P})\right)^{T}\left(\mathbf{V}^{*}_{cell} - \mathbf{V}_{cell}(\mathbf{P})\right) = \sum_{m=1}^{M}\sum_{n=1}^{N}\left(V^{*}_{cell,i} - V_{cell,i}(\mathbf{P})\right)^{2} \quad (3.7)$$

The aim of the PE method is (1) to minimize the objective function with a mathematical optimizer and (2) to determine the resulting unknown parameters (**P**):

$$\min S = S(\mathbf{P}) \; subject\,to\, P_{j,low} \le P_{j,1} \le P_{j,high} \quad (3.8)$$

$P_{j,low}$ and $P_{j,high}$ are the minimum and the maximum possible values of P_j respectively.

Stochastic techniques are well suited for inverse problems with many parameters in the objective function. These techniques are also recommended for functions that exhibit local minimums in the vicinity of a global minimum. This is why a Genetic Algorithm (GA) was adopted in Part I for estimating the large number of electrochemical parameters of the Li-ion battery.

3.5 The reference data and the parameters

3.5.1 The Reference data

The calculation procedure exemplified in Part I of this study will now be tested for three Li-ion batteries whose positive electrode is made of $LiCoO_2$ (LCO), $LiMn_2O_4$ (LMO) and $LiFePO_4$ (LFP) materials.

Experimental data for Li_xC_6/Li_yCoO_2 and $Li_xC_6/Li_yMn_2O_4$ materials were retrieved from the literature. The data for the Li_xC_6/Li_yFePO_4 cell were generated by standard galvanostatic charge/discharge tests on a commercial cell.

The experimental data of a pouch cell reported by Santhanagopalan *et al*. [34] were used as the reference data for the C/LCO cell. Charge and discharge tests were conducted for a carbon (MCMB) /LCO cell for rates of C/5, C/2, 1C, and 2C.

Experimental data for C/LMO cell are provided by the work of Doyle *et al*. [16]. Potential versus capacity curves are reported for discharge rates ranging from 0.1C to 4C.

Experimental data from a cylindrical 18650 graphite/LFP cell were employed for the validation of the PE procedure on LFP cells galvanostatic discharge curves at both low and high C-rates were used to find the physical and the electrochemical parameters.

The equations used for calculation open circuit potential (OCP) as a function of state of charge for graphite, LCO and LMO are given in Appendix. The open circuit potential of LFP positive electrode was calculated by interpolating the experimental data at low discharge current. Note that the open circuit potential is an intrinsic characteristic of each positive electrode material. The open circuit potentials are dependent upon the ionic intercalation/deintercalation mechanisms. As a result, the range of influence of the battery's parameters may change, hence the need to perform a sensitivity analysis for validating the PE procedure for various active materials.

3.5.2 The parameters

Numerous physical and chemical parameters are needed for simulating the behavior of Li-ion batteries and for predicting their performance. Some parameters such as the physical dimensions or the chemistry of materials are readily available from the manufacturer. Other parameters are more difficult to determine. These hard-to-get parameters include design parameters (porosity, particle size, etc.), electrode specific parameters (diffusion coefficients, electrical conductivity, contact resistance, etc.), and kinetics parameters (transfer coefficients, reaction-rate constants, etc.). Parameter estimation methods allow the determination of these parameters from experimental charge/discharge curves. For the present study, eight electrochemical parameters were determined with the parameter estimation method. These parameters are the solid diffusion coefficients ($D_{s,n}$ and $D_{s,p}$), the intercalation/deintercalation reaction-rate constants (K_n and K_p), the initial SOC ($SOC_{n,0}$ and $SOC_{p,0}$), and the electroactive surface areas (S_n and S_p). In spite of the fact that all these parameters are identifiable with the Li-ion direct model, their magnitude is dependent on the positive and negative materials. Table 3.1 provides some of their values reported in the open literature.

On the other hand, different active materials exhibit different behavior during charge/discharge processes. The chemical/electrochemical properties are influenced by the intercalation/deintercalation mechanisms and by the structure of the active materials. This behavior will be elucidated in the sensitivity analysis.

Table 3.1: Range of the diffusion coefficients and of the reaction rate constants for Li-ion batteries

Parameter	LCO	LMO	LFP
Diffusion coefficient, D_{Li} [m^2/s]	1.0e-14 [8,34]	1.0e-13 [16]	1.18e-18 [31]
Reaction rate constant, K [$m^{2.5}/mol^{0.5}$ s]	6.6667e-11 [8]	2.334e-11[53]	1e-13 [63]

Parameter	LFP			Graphite		
	low	high	Ref.	low	high	Ref.
Diffusion coefficient, D_{Li} [m^2/s]	10e-22	10e-14	[54-59]	9e-10	2e-10	[21,28,60-64]
Reaction rate constant, K [$m^{2.5}/mol^{0.5}$ s]	10e-13	10e-9	[31, 62,63, 65-68]	8.19e-12	5e-11	[61,63,68,69]

3.6 Sensitivity analysis

A sensitivity analysis may be conducted for delineating the time interval domain for which the output of the system, i.e., the cell potential, is most sensitive to the input parameters and the properties. The sensitivity analysis improves the accuracy of the inverse method and the parameter estimation process.

The sensitivity or the Jacobian matrix (**J**) is defined as the first order partial derivative of the calculated cell potential $\left(\boldsymbol{V}_{cell}(\boldsymbol{P})\right)$ with respect to the unknown parameters ($\mathbf{P}_j$), that is:

$$\mathbf{J}\left(\mathbf{P}_j\right)=\left[\frac{\partial \mathbf{V}_{cell}^{T}}{\partial \mathbf{P}_j}\right]^{T} \tag{3.9}$$

As explained in Part I, the governing equations for the SPM are employed to calculate the dimensionless sensitivity coefficients for each parameter. The sensitivity coefficients depend on time and on the discharge rate.

The discharge curves may be divided into three regions: 1. the early stages of the discharge process; 2. the intermediate region of the discharge process when the potential varies gradually; 3. the end of the discharge process characterized by a sharp decline in the potential. Farkhondeh *et al*. [70] fitted experimental data for Li/LFP half-cells for these three regions. The authors were able to determine the regions where each of the cell parameters is the most influential on the battery's behavior.

In the present study, the best time domain for the PE of different electrochemical parameters is determined from a sensitivity analysis of the electrode chemistry.

The best time domains for estimating the parameters of a graphite/$LiCoO_2$ cell are shown in Figure 3.2 (see also Figure 5f in Part I). Green and red colored parameters can be estimated better in low and high discharge rates, respectively. Therefore, the best time domain for estimating $D_{s,p}$ at low discharge rates is region 2, and region 3 for high discharge rates. It was concluded, in Part I, that $D_{s,n}$, K_n and K_p can be determined from region 2, for both low and high discharge rates. For all discharge rates, region 3 is best for determining S_n and $SOC_{n,0}$. Finally, regions 1 and 3 are the best time intervals to find S_p and $SOC_{p,0}$, at both low and high discharge rates

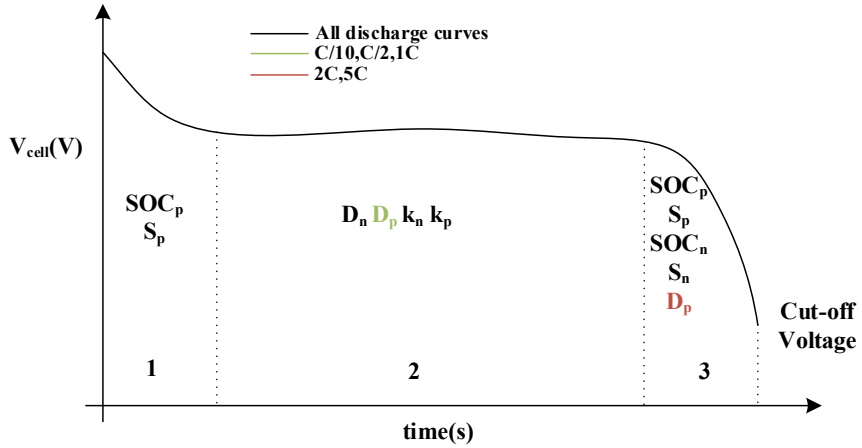

Figure 3.2: Schematic curve of sensitivity analysis for graphite/$LiCoO_2$ (presented in Part I)

The best time domains for estimating the parameters of the graphite/$LiMn_2O_4$ cell were obtained from a sensitivity analysis. The results are depicted in Figure 3.3. In this case, the discharge curve was divided into 2 regions. The main conclusions to be drawn from this figure are:

- For the parameters $SOC_{n,0}$, S_n, $D_{s,n}$, K_n and K_p: Region 1 appears to be the best time domain for both low and high discharge rates.
- For the parameter $D_{s,p}$: Region 1 is recommended for low discharge rates. Region 2 is better for high discharge rates.
- For the parameters S_p and $SOC_{p,0}$: Region 2 is best for both low and high discharge rates.

The sensitivity analysis also provides the order of sensitivity of the parameter, which is S_p, $SOC_{p,0}$, $SOC_{n,0}$, S_n, K_p, K_n, $D_{s,p}$, $D_{s,n}$. This order results from different Jacobian value for each parameter. For instance, it was found that the output cell potential is more sensitive to S_p than to $D_{s,n}$.

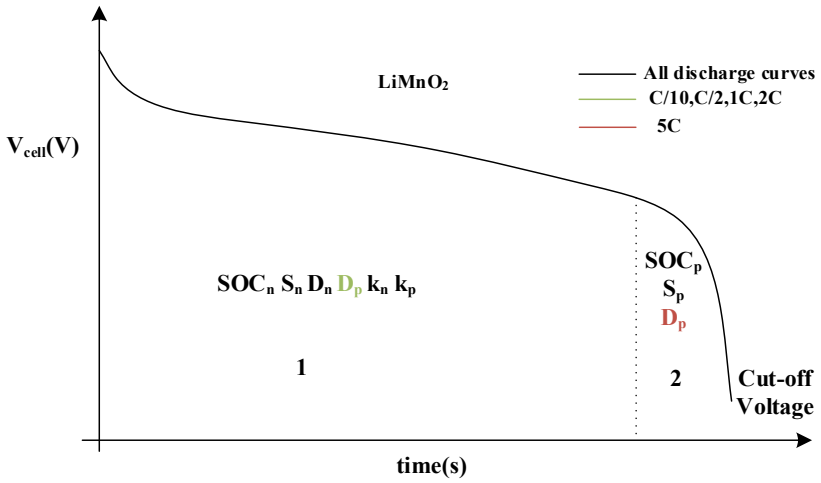

Figure 3.3: Schematic curve generated from a sensitivity analysis for graphite/$LiMn_2O_4$

A similar sensitivity analysis was conducted for graphite/$LiFePO_4$. The results are illustrated in Figure 3.4. The conclusions concerning the best time domains for estimating the parameters of this battery may be summarized as follows:

- For the parameters $D_{s,n}$, K_n and K_p: region 2 appears to be the best time domain for both low and high discharge rates.
- For the parameter $D_{s,p}$: Region 1 is recommended only for low discharge rates (C/10). The dimensionless sensitivity coefficient for $D_{s,p}$ is close to zero at other discharge curves.
- For the parameters ε_n and $SOC_{n,0}$: Region 3 is suitable at all discharge rates.
- For the parameters ε_p and $SOC_{p,0}$: Region 1 is prescribed for both low and high discharge rates.

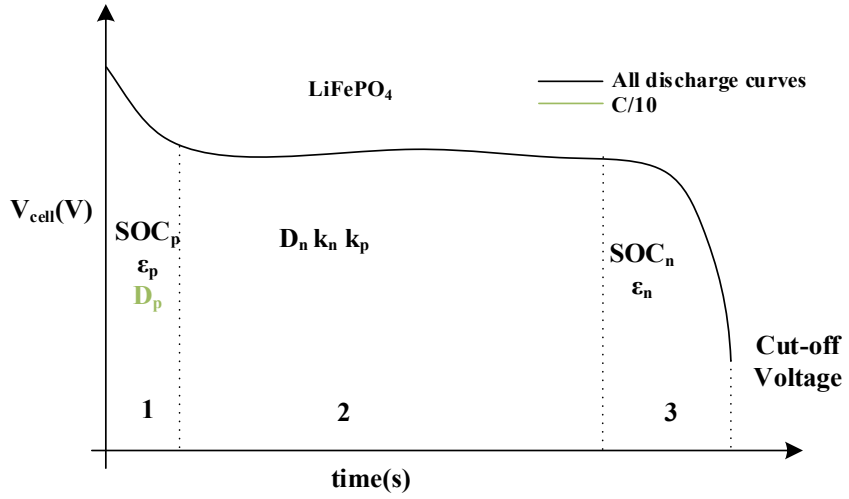

Figure 3.4: Schematic curve of sensitivity analysis for graphite/LiFePO4

The parameter sensitivity resulting from the PE analysis may be stated in the following decreasing order: $SOC_{n,0}$, ε_n, $SOC_{p,0}$, K_n, $D_{s,n}$, ε_p, K_p, $D_{s,p}$. This order reveals that the PE process for graphite material is more sensitive than that for LFP. This behavior is shown in Figure 3.5. The open circuit potential of the electrodes and the cell potential are compared.

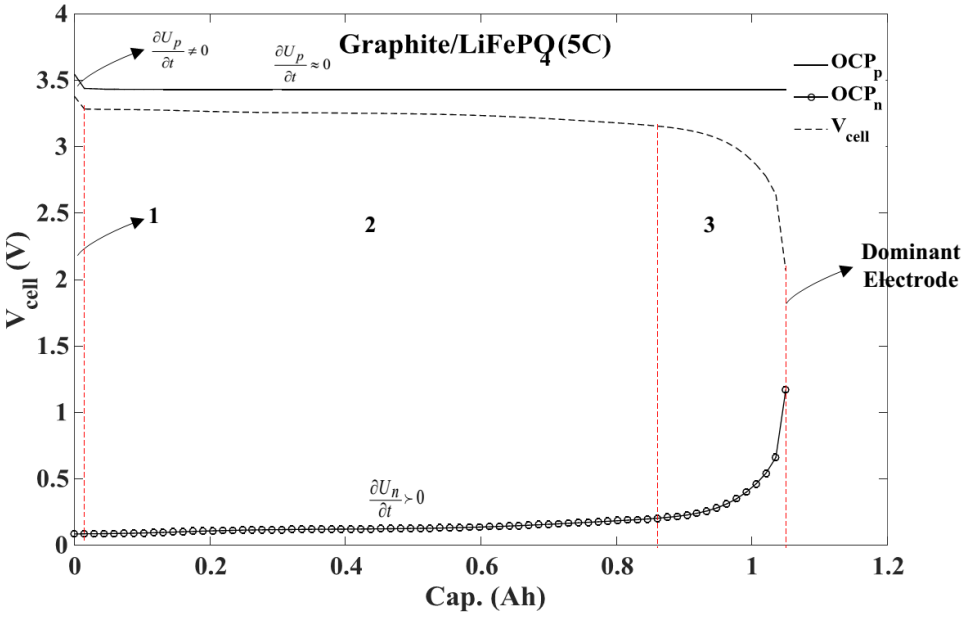

Figure 3.5: Cell potential and open circuit potential of two electrodes (graphite/LFP) for a discharge current of 5C

Figure 3.5 reveals that the cell potential follows the open circuit potential of the LFP in region 1 only. In regions 2 and 3, the LFP has no influence. Graphite is the dominant electrode. The LFP electrode is made of fine powder compared to that of graphite electrode. As a result, the capacity of the positive electrode is higher than that of the negative electrode when the thickness and the porosity of two electrodes are almost same. This is the case for graphite/LFP cells designed for high power applications. Here, the LFP electrode is almost always operated in the plateau region. Since graphite material dictates the overall potential, the effect of the LFP electrode on the performance of the graphite/LFP cell is insignificant.

Fortunately, for future studies such as introducing an aging model considering the changes in dominant parameters, PE methodology is still valid and helpful. Due to the fact that graphite is recognized as the most dominant electrode in losing capacity mechanisms. In addition, it is worth noting that the methodology is anticipated to be well capable to estimate the influential parameters of LFP positive electrode material when LFP is the dominant electrode with capacity less than graphite. In fact, in this case, the order of sensitivity of the potential to the parameters would change and parameters related to the capacity of the positive electrode such as diffusion coefficient and porosity would possess higher sensitivities.

In order to simulate graphite/LFP cell, a Mosaic model was developed [71]. The Mosaic model proposed by Andersson *et al*. was adopted [71]. This model assumes a particle-radius dependency on the current density. Small radius particles are involved in the lithiation/delithiation process at high current densities. Large radius particles are, on the other hand, influential at lower current densities. Maheshwari *et al*. [65] adjusted the radius of the positive electrode particles for each C-rate in order to match the simulation results with the experimental data. Maheshwari *et al*. concluded that employing a current dependent radius is equivalent to simulating the actual particle size distribution (PSD). Prada *et al*. [62] observed a similar behavior for the evolution of the particle radius with the current density. The higher the current density, the smaller is the effective particle radius. Prada *et al*. have developed a Mosaic model in which the radii of both positive and negative electrodes were adjusted according to the experimental data.

Here, the Mosaic model was used to simulate the discharge curves of LFP/graphite cells of the 18650 battery type. The model was applied to the negative electrode (the graphite electrode) so as to obtain a good fit between the numerical predictions and the experimental data.

3.7 Results and discussion

The inverse methodology introduced in Part I was implemented to find each parameter in its best time domain. The PE was carried out for different Li-ion batteries.

Table 3.2 presents the estimated parameters for the graphite/$LiCoO_2$ cell. Each parameter was calculated for its best time domain.

Table 3.2: Estimated parameters for the graphite/$LiCoO_2$ cell

Symbol	Units	Range		Estimated value
		min	max	
$D_{s,p}$	m^2/s	1.0e-15	1.0e-13	9.9451e-14
$D_{s,n}$	m^2/s	1.0e-15	1.0e-13	4.9270e-14
K_p	$m^{2.5}/mol^{0.5}$ s	1.0e-12	1.0e-10	4.1618e-11
K_n	$m^{2.5}/mol^{0.5}$ s	1.0e-12	1.0e-10	2.1138e-11
S_p	m^2	0.6	1.3	1.02
S_n	m^2	0.6	1.3	0.81
$SOC_{p,0}$	-	0.4	0.6	0.53
$SOC_{n,0}$	-	0.6	0.8	0.68

Figure 3.6 compares the predicted and the experimental discharge curves for different currents (C/5, C/2, 1C and 2C). The agreement between the simulation and the experiment is striking.

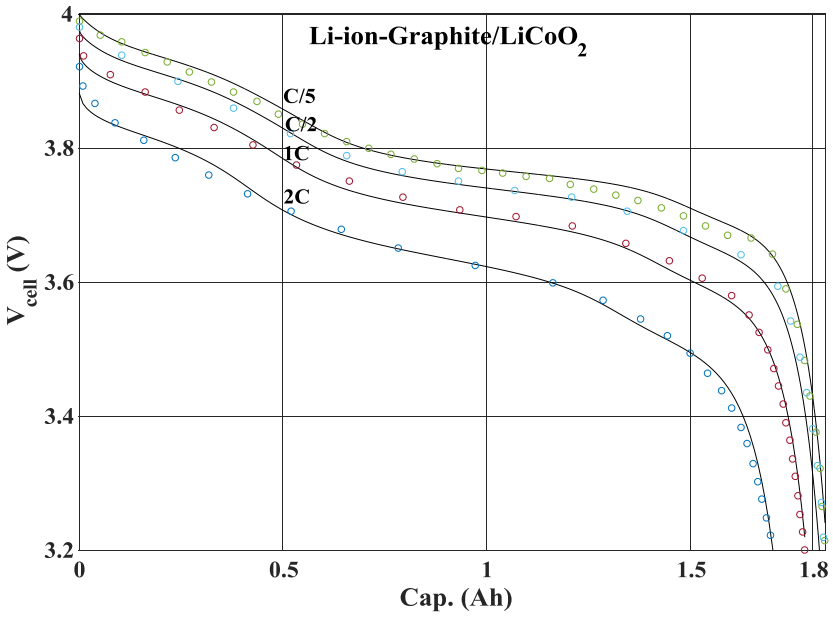

Figure 3.6: Simulated (solid lines) and experimental (symbols) discharge curves for the graphite/$LiCoO_2$ cell

The PE methodology developed in Part I was next tested for the spinel $LiMn_2O_4$ positive electrode. The estimated parameters are summarized in Table 3.3.

Table 3.3: Estimated parameters for the graphite/ $LiMn_2O_4$ cell

Symbol	Units	Range		Estimated value
		min	max	
$D_{s,p}$	m^2/s	1.0e-15	1.0e-12	6.7259e-13
$D_{s,n}$	m^2/s	1.0e-15	1.0e-12	7.5502e-13
K_p	$m^{2.5}/mol^{0.5}$ s	1.0e-12	1.0e-10	1.8324e-11
K_n	$m^{2.5}/mol^{0.5}$ s	1.0e-12	1.0e-10	2.8141e-11
S_p	m^2	0.9	1.6	1.39
S_n	m^2	0.9	1.6	1.42
$SOC_{p,0}$	-	0.17	0.3	0.22
$SOC_{n,0}$	-	0.65	0.85	0.71

Estimated parameters introduced in Table 3.3 were used as the input of simplified P2D model. Figure 3.7 confronts the predicted and the measured discharge curves. Once again, the numerical predictions match the experimental data.

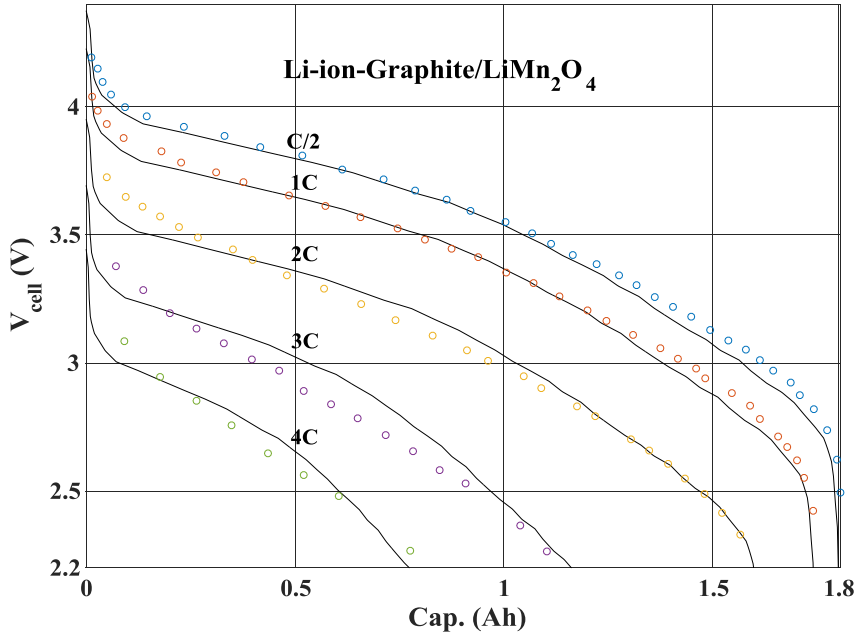

Figure 3.7: Simulated (solid lines) and experimental (symbols) discharge curves for the graphite/$LiMn_2O_4$ cell

Table 3.4 provides the estimated parameters for the graphite/LFP. The simulations were conducted using a current dependent radius for the negative electrode (based on the Mosaic model). In this case, the electroactive area is a dependent parameter (Eq. (3.2) and (3.3)). The porosities of the electrodes (ε_p and ε_n) were chosen as the estimated parameters instead of the total electroactive area of the electrodes.

Table 3.4: Estimated parameters for the graphite/$LiFePO_4$ cell

Symbol	Unit	Range		Estimated value
		min	max	
$D_{s,p}$	m^2/s	1.0e-19	1.0e-17	4.0064e-18
$D_{s,n}$	m^2/s	1.0e-16	1.0e-14	4.6450e-15
K_p	$m^{2.5}/mol^{0.5}$ s	1.0e-13	1.0e-11	9.2287e-12
K_n	$m^{2.5}/mol^{0.5}$ s	1.0e-12	1.0e-10	3.4281e-12
ε_p	-	0.3	0.45	0.39
ε_n	-	0.4	0.6	0.60
$SOC_{p,0}$	-	0.01	0.06	0.05
$SOC_{n,0}$	-	0.75	0.82	0.81

The Mosaic model was applied where the apparent radius of the graphite active material needed to be estimated from the discharge current. Figure 3.8 shows the decrease of particle radius as current increases.

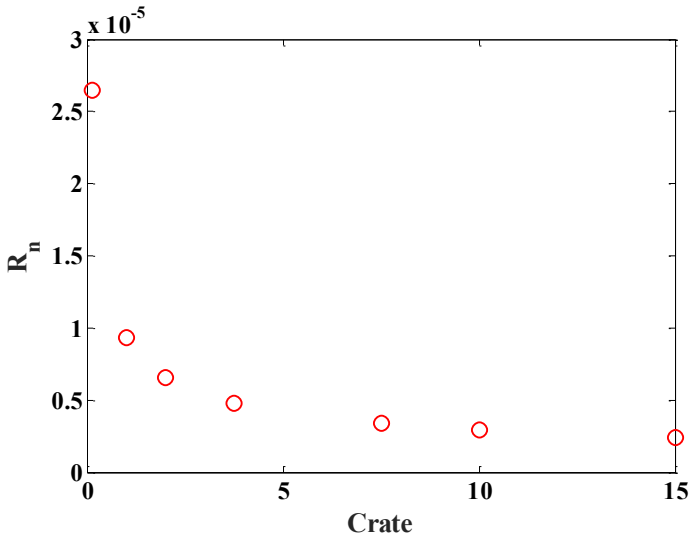

Figure 3.8: Current-dependent radius of particles in graphite electrode

Figure 3.9 depicts the simulated and the experimental discharge potentials of the cell. The accuracy of the mathematical model is validated at both high and low discharge rates.

It is common to check the risk of over-fitting in PE studies. This issue may happen when number of parameters in PE is large. In this case, inverse method finds the parameters that are more representatives of the noise of the system than the general trend. These set of parameters simulates the behavior of the cell perfectly, however they are unable to find the results in other conditions. To prevent this issue it is always better to find solutions that are more general. A strategy to examine over-fitting is to check the predictability of the model in a new condition

other than conditions that are used for PE. In Figure 3.9, simulated potential for discharge rate of 10C is provided by parameters estimated from lower discharge rates (mentioned in Table 3.4). It is obvious that the model is able to predict the performance of cell outside the conditions used for PE.

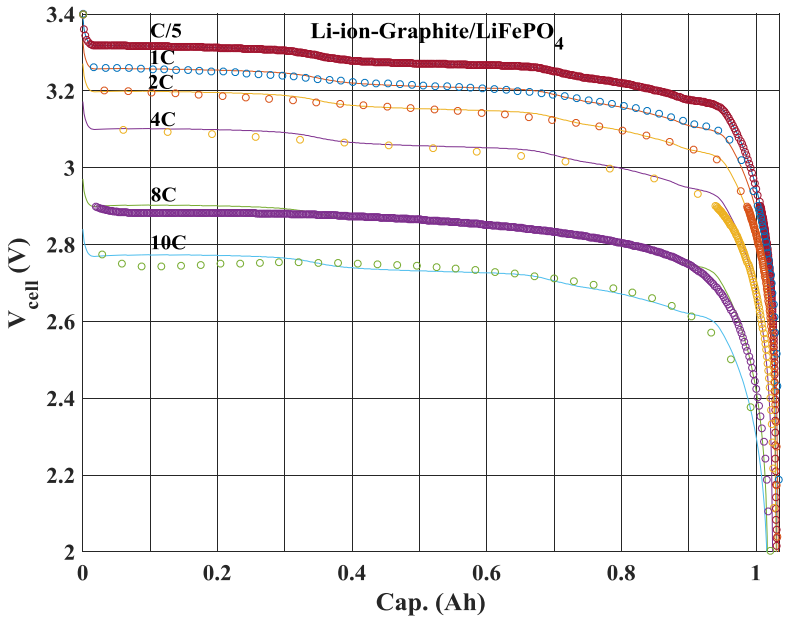

Figure 3.9: Simulated (solid lines) and experimental (symbols) discharge curves for the graphite/ $LiFePO_4$ cell

By using Eq. (10), the specific error values for each discharge curve is calculated for each cathode materials and presented in Table 3.5.

$$e_S = \left(\frac{1}{N}\right)\sum_{i=1}^{N}\left(V^{*}_{cell,m,i} - V_{cell,i}(\mathbf{P})\right)^2 \qquad (3.10)$$

Table 3.5: the specific error values of all discharge curves for each cathode material

e_s	C/5	C/2	1C	2C	3C	4C	8C
LiCoO2	1.1×10^{-4}	2.0×10^{-4}	1.0×10^{-4}	1.2×10^{-4}	-	-	-
$LiMn_2O_4$	-	1.0×10^{-4}	3.0×10^{-4}	1.1×10^{-3}	4.5×10^{-3}	1.0×10^{-2}	-
$LiFePO_4$	2.5×10^{-6}	-	4.1×10^{-5}	1.5×10^{-4}	-	8.4×10^{-4}	1.5×10^{-3}

3.8 Conclusion

A methodology for the electrochemical Parameter Estimation (PE) of Li-ion batteries was developed. The methodology rests on an inverse method combined to a simplified version of the Pseudo-two-Dimensional (P2D) model. It is designed to identify the solid diffusion coefficients ($D_{s,n}$ and $D_{s,p}$), the intercalation/deintercalation reaction-rate constants (K_n and K_p), the initial SOC ($SOC_{n,0}$ and $SOC_{p,0}$), and the electroactive surface areas (S_n and S_p) of the Li-ion battery. The methodology was tested for $LiCoO_2$, $LiMn_2O_4$ and $LiFePO_4$ positive electrode materials. The numerical predictions showed excellent agreement with the experimental data in all cases.

Acknowledgements

The authors are very grateful to Hydro-Québec and to the Natural Sciences and Engineering Council of Canada (NSERC) for their financial supports.

Appendix

Guo *et al*. fitted the experimental curves to find open circuit potential for Li_yCoO_2 as a function of the state of charge (SOC) in the following manner [8]:

$$U_{LCO} = 4.04596 + \exp\left(-42.30027 \times SOC_p + 16.56714\right) - 0.04880 \arctan\left(50.01833 \times SOC_p - 26.48897\right) - 0.05447 \arctan\left(18.99678 \times SOC_p - 12.32362\right) - \exp\left(78.24095 \times SOC_p - 78.68074\right) \quad (3.11)$$

Where the surface state of charge of the positive electrode (SOC_p) equals to the stoichiometric value *y* in Li_yCoO_2.

Open-circuit potential of LMO can be calculated in terms of the SOC from the following curve fitting equation [16]:

$$U_{LMO} = 4.19829 + 0.0565661 \tanh\left[-14.5546 \times SOC_p + 8.60942\right] - 0.0275479\left[\frac{1}{\left(0.998432 - SOC_p\right)^{0.492465}} - 1.90111\right] - 0.157123 \exp\left(-0.04738 \times SOC_P^8\right) + 0.810239 \exp\left[-40\left(SOC_p - 0.133875\right)\right] \quad (3.12)$$

Where SOC_p equals to the stoichiometric value y in $Li_yMn_2O_4$.

The open circuit potential of the negative electrode was expressed in terms of the SOC [8]:

$$\begin{aligned} U_{LiC_6} &= 0.13966 + 0.68920\exp\left(-49.20361\times SOC_n\right) + 0.41903\exp\left(-254.40067\times SOC_n\right) \\ &-\exp\left(49.9788\times SOC_n - 43.37888\right) - 0.028221\arctan\left(22.52300\times SOC_n - 3.65328\right) \\ &-0.01308\arctan\left(28.34801\times SOC_n - 13.43960\right) \end{aligned} \tag{3.13}$$

Where the surface state of charge of the negative electrode (SOC_n) equals to the stoichiometric value x in Li_xC_6.

Nomenclature:

$c_{s,k}^{\max}$	Maximum concentration of Li^+ in the particle of electrode *k (k=p,n)*, mol/m^3
$c_{s,k}^{surf}$	Concentration of Li^+ at the surface of the particles of the electrode *k (k=p,n)*, mol/m^3
$D_{s,k}$	Li^+ diffusion coefficient in the particle of electrode *k (k=p,n)*, m^2/s
F	Faraday's constant, C/mol
I	Applied current density, A/m^2
J_{pj}	Dimensionless sensitivity coefficient, V
K_k	Reaction rate constant of electrode *k (k=p,n)*, m$^{2.5}$/mol$^{0.5}$s
n	Negative electrode
p	Positive electrode
P	Unknown parameter matrix
r	Radial coordinate, m
R	Universal gas constant, J/mol K
R_k	Radius of the particle of electrode *k (k=p,n)*, m

S	Objective function, V^2
S_k	Total electroactive area of electrode *k (k=p,n)*, m^2
SOC_k	State Of Charge of electrode *k (k=p,n)*
$SOC_{k,0}$	Initial State Of Charge of electrode *k (k=p,n)*
t	Time, s
T	Absolute temperature, K
U_k	Open-circuit potential of electrode *k (k=p,n)*, V
V_k	Total volume of electrode *k (k=p,n)*, m^3
$\mathbf{v}_{cell}$	Numerical potential, V
$\mathbf{v}^*_{cell}$	Experimental potential, V
x	Spatial coordinate, m
x	Stoichiometric coefficient of Li in negatove electrode
y	Stoichiometric coefficient of Li in positive electrode

Greek

ε_k	Porosity of region *k (k=p,s,n)*

CHAPITRE 4 : AVANT-PROPOS

Auteurs et affiliation:

- Barzin Rajabloo: étudiant au doctorat, Université de Sherbrooke, Faculté de génie, Département de génie chimique et de génie biotechnologique.
- Ali Jokar: étudiant au doctorat, Université de Sherbrooke, Faculté de génie, Département de génie chimique et de génie biotechnologique.
- Walter Wakem Fankem: étudiant à la maîtrise, Université de Sherbrooke, Faculté de sciences, Département de chimie.
- Martin Désilets: professeur, Université de Sherbrooke, Faculté de génie, Département de génie chimique et de génie biotechnologique.
- Gessie Brisard: professeur, Université de Sherbrooke, Faculté de sciences, Département de chimie.

Revue: The Journal of Power Sources

Titre français: Un nouveau modèle SPM (Modèle à particule unique) avec résistance variable représentant les électrodes à base de Fer-Phosphate

Contribution au document: Cet article contribue au développement d'un nouveau modèle SPM (Modèle à particule unique) qui représente fidèlement le comportement spécifique des piles au Li-ion à base d'électrodes positives de Fer-Phosphates.

Résumé français : Une nouvelle approche empirique basée sur l'utilisation d'une résistance variable est proposée pour le modèle SPM (Modèle à particule unique) afin de représenter la faible conductivité électronique et ionique des électrodes positives à base de Fer-Phosphate des piles au Li-ion (LFP). L'augmentation de résistance observée dans les piles LFP en fin de décharge peut être expliquée par deux phénomènes : 1. Une augmentation de la surtension associée au transfert de masse qui résulte du phénomène d'intercalation/désintercalation des ions dans les plus grosses particules. 2. L'augmentation de la résistance ohmique basée sur la caractéristique bien connue des piles LFP, appelée « resistive-reactant ». Le nouveau modèle a été validé à partir de données expérimentales obtenues à l'aide de 2 types de piles-bouton fabriquées en laboratoire: un type haute énergie et un type haute puissance. Une comparaison entre les résultats expérimentaux et les prédictions du modèle numérique montre que le nouveau modèle à résistance variable représente adéquatement l'augmentation de résistance en fin de décharge pour ce type de piles au Li-ion.

4. A new variable resistance single particle model for lithium iron phosphate electrode

4.1 Abstract

Based on the poor intrinsic ionic and electronic conductivity features of lithium iron phosphate (LFP), an empirical variable resistance approach is proposed for the Single Particle Model (SPM). The increasing resistance behavior observed at the end of discharge process of LFP batteries can be justified by two phenomena: 1. Increasing diffusion overpotential that results from the intercalation/deintercalation of ions in larger particles. 2. Increasing ohmic resistance based on the resistive-reactant feature of LFP as the positive electrode active materials. The model is validated for two different laboratory made Li/LFP coin cells: a high-energy and a high-power configuration. Comparisons between the experimental results and the model predictions reveal that a variable resistance is successful to tackle the increasing overpotential.

Keywords: Single particle model (SPM), Lithium iron phosphate (LFP), Parameter estimation.

4.2 Introduction

The high thermal stability and safety as well as the high reversibility of olivine $LiFePO_4$ have made it the most promising material for the positive electrode of Li-ion cells, especially for applications in electric vehicles. However, some improvements are still necessary to overcome some of its deficiencies, such as poor electronic conductivity [72, 73] and low apparent lithium diffusivity [74, 75].

The poor intrinsic ionic and electronic conductivity of this material have been improved by decreasing the size of the LFP powder to the nanoscale and by adding a carbon coating upon the surface of the particles, respectively [73, 75, 76].

Another specific behavior of the LFP active material is its electrochemical delithiation reaction, which is occurring through a two-phase process [77]. It is generally accepted that during the intercalation/deintercalation of the Li ion, lithium iron phosphate undergoes a two-phase mechanism where the existence of both Li-poor Li_xFePO_4 and Li-rich $Li_{1-y}FePO_4$ phases results in a stable voltage plateau at 3.5V [78].

There are different approaches to simulate the complex behavior of LFP including the core-shell [66, 79-82], the phase field [83-85], the domino cascade [86], the spinodial decomposition [85, 87], the resistive-reactant (RR) [31, 63, 88], the variable solid-state diffusivity (VSSD) [70, 89,

90] and the mosaic models [71]. Different explanations are proposed to justify the disagreements between the aforementioned models [91]: the specific experimental conditions and the dependency of delithiation/lithiation kinetics and phase compositions on the particle size, the morphology and physical properties of the studied $LiFePO_4$ material, to name a few.

Srinivasan and Newman [66] developed a core-shell model initially introduced by Padhi *et al*. [79]. Intercalation and phase change in LFP were both represented through a shrinking core model consisting of a Li-rich and a Li-poor phases. The diffusion of Li inside the growing shell of one phase (e.g. Li-rich phase of $LiFePO_4$ during discharge) and the mass transfer across the phase boundary to the core of the other phase (e.g. Li-poor phase of $FePO_4$ during discharge) were addressed in their model.

Although the treatment of the two-phase process considered in core-shell, phase-field, domino cascade and spinodial decomposition models may be appropriate to simulate galvanostatic discharge of the Li-ion cell, it requires important computational resources when simulating cycling working conditions. Less demanding models such as VSSD which somehow simulate the influence of the phase change without considering it explicitly [70], on the other hand, are among best candidates for large-scale applications of secondary batteries such as battery management systems.

Thorat made an effort to find an alternative and easier way to represent the influence of the aforementioned two-phase process [89]. He introduced a model with a concentration-dependent solid-state diffusion coefficient for LFP. However, he had to use the Fickian diffusion with a constant solid-state diffusivity to obtain results that are more representative of the battery performance.

Later, in 2012, Farkhondeh and Delacourt [90] improved the approach of Thorat [89] to simulate different commercial LFP electrodes. They introduced a variable solid-state diffusivity (VSSD) model while ignoring the porous-electrode effects. To make the model suitable for high C-rates, Farkhondeh *et al*. [70] merged the VSSD model with the pseudo-2-dimensional (P2D) model of Doyle *et al*. [49]. They also considered a particle sizes distribution (PSD) for the active material, taking into consideration 4 different particle sizes. Although the VSSD model of Farkhondeh *et al*. [70] exhibited good simulation results, it is not appropriate for large scale and heavy simulations like the ones involved in the simulation of battery packs.

The mosaic model, proposed by Andersson *et al*. [71], is a low-cost approach that accounts for a distribution of particle sizes of the active material (PSD). This model is based on the particle-radius dependency on the current density. More precisely, when the current density is high, the particles with smaller radius are more active in lithiation/delithiation mechanism. Large radius particles are, on the other hand, more influential at lower current densities. Later, the mosaic

model has been implemented by others [40, 45, 62, 65, 92] to improve the predictability of the model vis-a-vis the capacity of LFP electrode material.

As mentioned earlier, another feature of the LFP electrode is its resistive-reactant behavior. LFP has the properties of an electrically insulating material [93]. Therefore, the use of conducting additives such as carbon is vital to decrease the ohmic drop and to improve the intrinsic electronic conductivity of LFP [94]. Quality and quantity of these conducting additives are at the origin of two different resistances: intraparticle and interparticle, respectively. The former represents the ohmic drop caused by the electrons travelling through non-carbon coated active-particle surface [88]. The later happens when the electrode is composed of poorly connected particles, which causes higher resistivity paths through the conductive matrix [63].

Thomas-Alyea [88] investigated the intraparticle resistivity of LFP by conducting experiments where two electrodes with a different amount of conductive carbon coating are compared. She concluded that the voltage drop in both charge and discharge profiles is due to intraparticle resistivity of LFP rather than the ionic conductivity of electrolyte and the electronic conductivity of the bulk positive electrode. Later, Safari and Delacourt [63] studied the interparticle resistance of LFP active material. They used a different number of current collectors at the anode side as a spacer to change the uniaxial pressure. In their experiments, they showed that increasing the uniaxial pressure improves the connectivity between the active material particles and thus decrease the ohmic drop due to the interparticle resistivity.

In their RR model introduced to simulate LFP, Safari and Delacourt [63] assumed four spherical particle groups with the same particle size but with different electronic connectivities to the conductive matrix. It should be noted that both interparticle and intraparticle resistances of LFP active material cause ohmic drop and consequently make a non-uniform current distribution. RR model has also been applied by others [70, 90] to consider the resistive-reactant feature of LFP.

Although VSSD and RR models seem good approaches to simulate the slow solid-state Li ion transport and the poor electronic conductivity of LFP, they are still not well suited to investigate cycling conditions and performing time-consuming studies such as aging and battery pack level simulation. Aiming at introducing a simple model to take into account the resistive reactant feature of LFP, Marcicki [95] combined his simplified Li-ion battery model with a resistance that varies linearly with the depth of discharge (DOD). He used the middle portion of the discharge curve to find a semi-empirical equation for resistive reactant effects. The results show a good agreement comparing with experimental data obtained from a cylindrical graphite/iron phosphate cell for a range of galvanostatic discharge experiments from C/3 to 4.8 C. However, there is also a need to study the resistive reactant effect of LFP in the whole portion of

discharge/charge curves of a Li/LFP half-cell, thus eliminating the influence of graphite as the negative electrode.

In this work, we introduce an improved varying resistance SPM and we apply it to study a Li/LFP half-cell. The exponential resistance introduced here shows promising results in simulating LFP material behavior. We examine the validity of the model for two different Li/LFP cells, a high-capacity and a high-power cells.

In the following sections, the experimental setup is presented. Afterward, the model development and its constitutive equations are explained. Finally, the results are discussed.

4.3 Experimental

Experimental studies were performed on a Li ($Li/LiFePO_4$) CR2032 coin cell made of commercial available positive and negative electrode materials. These coin cells were built by assembling the following components (see Figure 4.1a): a positive electrode, a negative electrode, a polypropylene separator membrane (Celgard 2400) between both electrode, a stainless steel spacers and a spring. Two different kind of cells were built: a high energy and a high power Li cells. Positive electrode is thicker (100 μm) in the high-energy Li cell than the high-power Li cell (34 μm).

The positive electrode was prepared using 85 % $LiFePO_4$/C, 7.5 % Carbon Black (CB) and 7.5 % PVDF (Polyvinylidene difluoride). The PVDF binder was first dissolved in N-methyl-2-pyrrolidinone. The mixture of $LiFePO_4$/C and carbon black was then added to the binder solution after being ball milled for 10 minutes. The slurry obtained was mixed using a magnetic stirrer for one hour in order to homogenize the mixture. The positive electrode was then cast, applying the slurry on one side of a sandblasted aluminum foil (25 μm thick). The treated electrode dried in an oven at 90 ^{o}C under vacuum (25 In Hg) for 6 hours. After drying, the positive electrode was calendared in order to reduce the porosity of the coating and finally punched in 2 cm^2 disks.

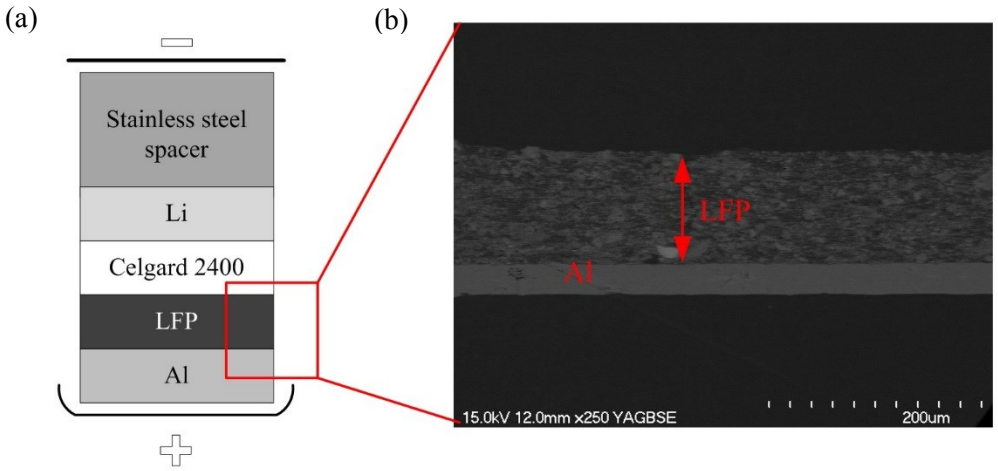

Figure 4.1: (a) Schematic of the cell (b) SEM image of the cross section of the positive electrode and current collector cross section

The electrolyte was prepared inside an argon-filled glove box (1 ppm H_2O) and consists of 1 M $LiPF_6$ salt in Ethylene Carbonate (EC), Dimethyl Carbonate (DMC) and Ethyl Methyl Carbonate (EMC), in a volume fraction of 1/1/1. All battery grade carbonates and Li salt have been bought from Sigma Aldrich.

The particle size distribution measured by laser diffraction sizing revealed that the mean value for the radius of particle is 0.35 μm. This value is considered as the radius of particle in 1-C discharge rate. Moreover, the specific area of the samples was studied using the Brunauer-Emmett-Teller method (BET).

Charge/discharge curves were measured using a MTI cycler BST8-MA. The BST8-MA cycler has been used to analyze the rate performance of the materials at different C-rate considering a cut-off voltage of 2.8-3.6 V. The charge consists of a Constant Current Charge (CCC) up to 3.6 V, followed by a Constant Voltage Charge (CVC) until the current reach the one corresponding to C/50. On the other side, the discharge consists of a simple Constant Current Discharge (CCD), down to a cut-off voltage of 2.8 V. Once assembled, the cells were subjected to SEI formation. The SEI formation consists of 5 cycles at low C-rate (C/12) in order to form a stable solid electrolyte interface.

4.4 Model development

Pseudo-two-dimensional (P2D) model [10, 16, 17, 49] is well suited for most simulations of Li-ion batteries because such a model is considering the mass transport and the charge transfer in both solid and electrolyte phases. However, the single particle model (SPM) [6-8], used as a simplified version of P2D, is a better candidate for simulating cycling conditions or other time-

consuming studies. The current distribution along the thickness of the porous electrode remains uniform in SPM, which is the case of Li-ion batteries with thin and highly conductive electrodes subjected to low current densities [8].

When it comes to fit the end-of-discharge capacity for LFP, SPM and P2D models give poor predictions, both assuming a constant diffusion coefficient in the solid active material ($D_{s,p}$) or a constant radius of the active material (R_p). In other words, constant value of $D_{s,p}$ (or R_p) may result in a good fitting for a specific current density. However, it leads to either under-prediction or over-prediction of utilization when higher or lower current densities are simulated [66]. This is a case where a rate-dependent diffusion coefficient [96, 97] or a rate-dependent radius of particle [40, 45, 62, 65, 92] can be implemented to obtain a representative end-of-discharge capacity. The Mosaic model is based on a rate-dependent radius of particle. The radius considered is typically increased when the discharge current goes from a higher value to a lower value. The mosaic model predicts the utilisation window of LFP active material very well, which is an indirect effect of the particle-size distribution (PSD) [65].

Figure 4.2 schematically compares the results of P2D and SPM with the experimental data for the discharge of the LFP half-cell (Li/LFP). Potential is depicted as a function of depth of discharge (DOD) in an arbitrary discharge rate higher than 1C. Here, the assumption is that both models are combined with a Mosaic model. Figure 4.2 reveals three important features: 1. the slope in the plateau region, 2. the end-of-discharge capacity, and 3. the increasing polarization as the discharge proceeds, especially at the end of the discharge process. In the case of the thin electrode, both SPM and P2D predict the performance reasonably well, mainly because of the uniform current distribution. However, in the case of the thick electrode, where a non-uniform current distribution exists, only P2D model can represent the slope of the discharge curve and the voltage drop due to the low conductivity of the matrix.

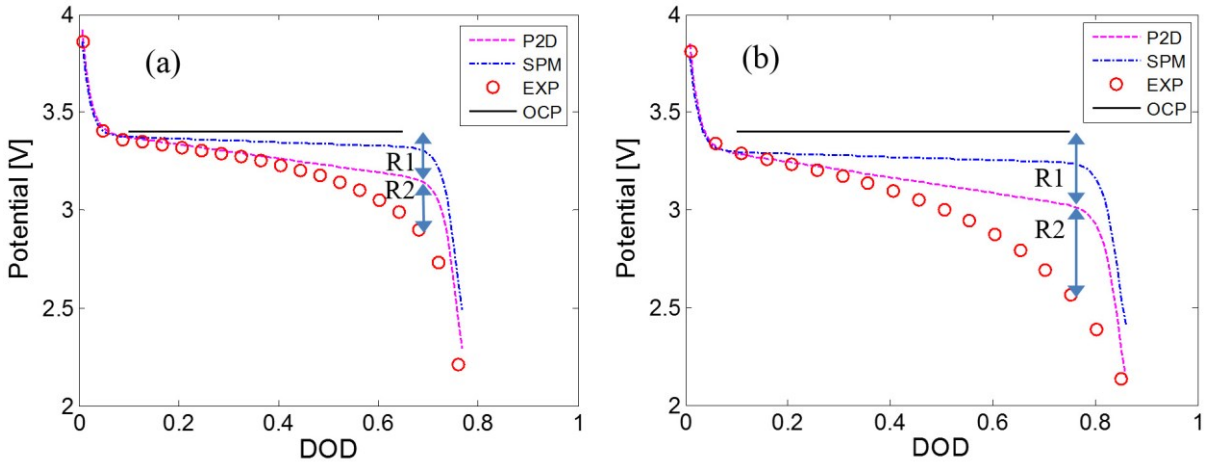

Figure 4.2: Schematic of the simulated and experimental discharge curves of Li/LFP half-cell with (a) thin positive electrode, and (b) thick positive electrode. OCP is depicted in its plateau condition.

For both models, the use of the Mosaic model helps to predict the end-of-discharge capacity. However, both models are unable to follow the increasing polarization at the end of the discharge. This is the place where other models such as the shrinking core, the VSSD or the RR models can be implemented to simulate this specific behavior of the LFP electrode active material. Srinivasan and Newman [66] divided the resistance into two components: 1. Contact, matrix and kinetic resistance (R_1 in Fig. 2), 2. Diffusion resistance (R_2 in Fig. 2). They showed promising results in simulating LFP positive electrode. Safari and Delacourt [63] and later Farkhondeh and Delacourt [70] attributed the resistance (R_1+R_2 in Fig. 2) to the resistive reactant feature of LFP and variable solid diffusivity of this active material. However, as described later, a model implementing a variable resistance function can produce good results without the necessity of using sophisticated and time-consuming models.

The cell resistance evolution during the charge/discharge process can be interpreted by comparing the flat OCP of LFP in intermediate SOC with the sloped voltage versus capacity curves at higher charge/discharge rates [63]. This resistance sums up the influences of the variable solid diffusivity as well as the resistive-reactant feature of LFP, including both interparticle and intraparticle resistances in following ways. First, assuming that smaller particles lithiate faster that the larger ones justifies increasing the transport limitation as the charge/discharge proceeds. Therefore, instead of using a variable diffusivity of ions into the solid active material to mimic a higher diffusion overpotential at the end of the charge/discharge, it is easier to integrate the mass transport limitations into a varying resistivity.

Moreover, as the charge/discharge proceeds, electrons and ions have to go through a larger distance inside the low conductive matrix phase [66]. Therefore, increasing the resistance during the end of discharge results from lithiating poorly coated particles (interaparticle resistance) and

poorly connected particles to the matrix (interparticle resistance). This behavior represents the resistive-reactant feature of LFP.

Another explanation for a varying resistance can be interpreted from Figure 4.3a where a discharge process is depicted schematically. Here, the potential as a function of DOD is compared with the OCP and the corresponding end of discharge capacity is also marked. The end of discharge clearly occurs when the OCP is still in the plateau region. This conclusion is based on a XRD (X-ray diffraction) analysis of a two identical cells: one discharged with C/24 rate and the other with 1C rate up to the cut off potential of 2.8 V (Figure 4.3b). The XRD diagram demonstrates that two phases are present in the disassembled LFP electrode after a 1C discharge rate. In other words, the end of discharge is reached before LFP active material gets homogeneous. Therefore, increasing overpotential at the end of discharge comes from another source of resistivity than high overpotential at one phase region of OCP. As a conclusion, an increasing resistance helps to introduce a simple and applicable model for LFP active material.

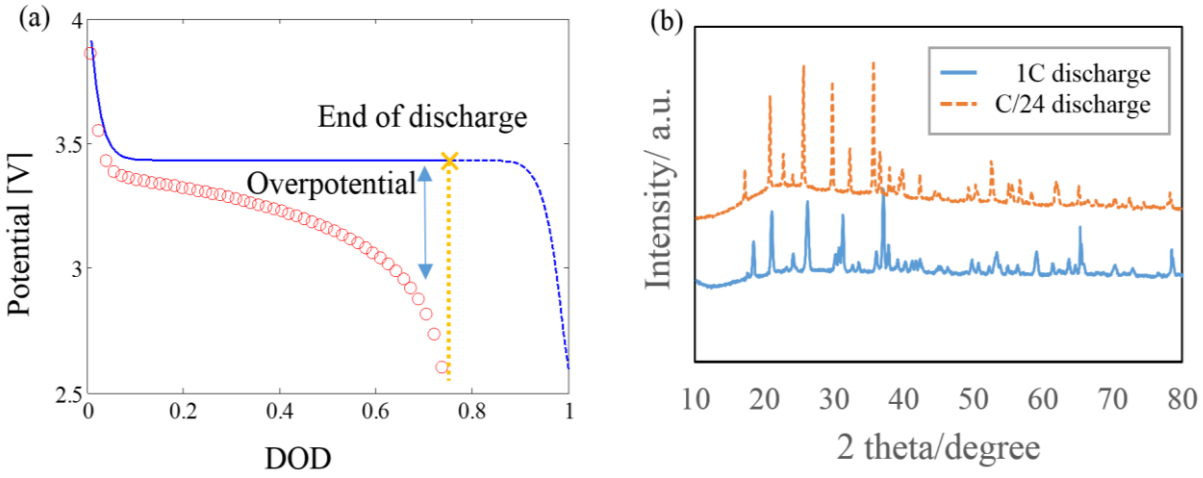

Figure 4.3: (a) Schematic of an experimental discharge potential and corresponding OCP, and (b) XRD analysis of disassembled LFP electrode after discharge process. Two phases exist in LFP active material discharged with 1C rate.

Such a varying resistance can be implemented into a single particle model (SPM) to build a more rapid and robust model, aimed at performing heavy simulations (for instance to study BMS or aging), for a large range of C-rates. It should be noted that there is no need for an electrolyte potential drop function [40, 45] because such resistive losses will also be included in the empirical varying resistance.

Assuming a uniform current distribution along the thickness of the porous electrode in SPM makes it possible to represent the entire porous electrode (positive/negative) by a single

intercalation particle [8]. Fick's second law in spherical coordinate system represents the mass balance of lithium ions in the electrode active material [8]:

$$\frac{\partial c_{s,j}}{\partial t} = \frac{1}{r^2}\frac{\partial}{\partial r}\left(D_{s,j} r^2 \frac{\partial c_{s,j}}{\partial r} \right) \tag{4.1}$$

with initial conditions as

$$c_{s,j}\left(t = 0, r\right) = c_{s,j}^{0} \tag{4.2}$$

The boundary conditions are zero flux of lithium ions at the center of the spherical particle (symmetry condition) and J_j molar flux of lithium ions at the surface of particle. These conditions can be expressed respectively as

$$D_{s,j}\left.\frac{\partial c_s}{\partial r}\right|_{r=0} = 0 \tag{4.3}$$

$$-D_{s,j}\left.\frac{\partial c_s}{\partial r}\right|_{r=R_j} = J_j \tag{4.4}$$

Where j = p, n for the positive and negative electrodes respectively, D_s is the solid phase lithium ion diffusion coefficient, and R_j is the solid particle radius.

The molar flux of lithium ions in SPM is related to total current I passing through the cell as

$$J_j = \frac{I}{FS_j} \tag{4.5}$$

Where F is Faraday constant and S_j is the total electroactive surface area of electrode j

$$S_j = \frac{3\varepsilon_j V_j}{R_j} \tag{4.6}$$

Where ε_j is the volume fraction of solid phase active material in electrode j and V_j is the total volume of that electrode. In the case of Li/LFP half-cell, the electroactive surface area of the negative electrode, S_n, is equal to the geometrical surface of the Li foil, A_n.

The state of charge (SOC) for the positive electrode is defined as

$$SOC_p = \frac{c_{s,p}}{c_{s,p,\max}} \tag{4.7}$$

Guo *et al*. [8] illustrated that Eq. (4.1) can be solved by Eigenfunction Expansion Method (EEM). They indicated that a mass balance on lithium ions in an intercalation particle of electrode active material yields the SOC at the surface of particle as [8]:

$$SOC_p = SOC_{p,ini} + \delta_p \left[3\frac{D_{s,p}}{R_p^2} t + \frac{1}{5} - \frac{2}{\lambda_k^2} \sum_{k=1}^{\infty} \exp\left(-\frac{\lambda_k^2 D_{s,p}}{R_p^2} t \right) \right] \tag{4.8}$$

Where δ_p is the dimensionless flux of lithium ions at positive electrode:

$$\delta_p = -\frac{I R_p}{S_p F D_{s,p} c_{s,p}^{\max}} \tag{4.9}$$

and λ_k is the k^{th} eigenvalue calculated from:

$$\sin \lambda_k - \lambda_k \cos \lambda_k = 0 \tag{4.10}$$

Once the SOC in positive electrode is known, the potential of the cell can be found as following:

$$m_p = \frac{I}{FK_p S_p c_{s,p}^{\max} c_e^{0.5} \left(1 - SOC_p\right)^{0.5} \left(SOC_p\right)^{0.5}} \tag{4.11}$$

$$m_n = \frac{I}{FK_n S_n c_e^{0.5}} \tag{4.12}$$

$$V_{cell} \approx U_p + \frac{2RT}{F} \ln\left(\frac{\sqrt{m_p^2 + 4} + m_p}{2} \right) + \frac{2RT}{F} \ln\left(\frac{\sqrt{m_n^2 + 4} + m_n}{2} \right) + I \times R_{cell} \tag{4.13}$$

In the potential equation (Eq. (4.13)), R_{cell} is the variable resistance function. Unlike other studies that consider a lumped resistance or a concentration dependent resistance, here a SOC dependent resistance is introduced to calibrate the SPM. Here, an exponential resistivity is introduced to account for increasing ohmic losses and diffusion overpotential as the discharge proceeds. The exponential form comes from the difference between the potential profile and OCP curve (see Figure 4.3a):

$$R_{cell} = a_1 \exp(a_2 \times SOC_p) + a_3 \tag{4.14}$$

The physical/electrochemical parameters and the unknown of cell variable resistance (Eq. (4.14)) are estimated by virtue of Parameter Estimation (PE) process [40, 45]. These parameters are the solid diffusion coefficient ($D_{s,p}$), the intercalation/deintercalation reaction-rate constant (K_p), the porosity of the electrode (ε_p), the unknown coefficients in the cell resistance equation (a_1, a_2 and a_3) and the radius of the particles at each discharge current except 1C. The radius of the particles for the 1C charge/discharge process is assumed 0.35 μm, based on particle size distribution.

4.5 Results and discussion

Two different types of coin cells were built in laboratory to examine the validity of the proposed model for both high-power and high-energy configurations. The thicknesses of the positive electrode of these configurations were measured from SEM: the high-power thinner electrode is 34 μm thick while the high-capacity thicker electrode is 100 μm thick. For a discharge rate of 1C, the assumed mean radius of particles is 0.35 μm. This value is measured with a laser diffraction-sizing instrument. However, the particle size has been estimated for other discharge rates, as it is proposed in the Mosaic model.

The open circuit potential (OCP) for each type of cells was determined from a discharge experiment at low C-rate (C/24). The rate constant (K_n) was assumed from an exchange current density of $i_n = F K_n c_e^{0.5} = 1.90\,\text{mA/cm}^2$, as reported in the literature [31] for similar technology. Table 4.1 provides the parameter values used for LFP and Li.

Table 4.1: Measured and assumed parameters for the Li// $LiFePO_4$ cell

Parameters	Positive electrode		Negative electrode	
	Symbol	Value	Symbol	Value
Electrode thickness (μm)		34[a] h.-power 100[a] h.-energy		
Particle radius for 1C (μm)	R_p	0.35[a]		
Maximum solid-phase lithium concentration (mol/m^3)	$c_{s,p}^{max}$	22,806[b][31]		
Exchange current density (mA/cm^2)			i_n	1.90[31]
Charge transfer coefficient	β_p	0.5[b]	β_n	0.5[b]
Salt concentration in the liquid phase (mol/L)	c_e	1[b]	c_e	1[b]

[a] Measured
[b] Assumed

The other parameters are estimated by virtue of the Parameter Estimation (PE) process. Table 4.2 presents the estimated parameters and the range used for each of them during the identification iterative process.

Table 4.2: Estimated parameters for the high-power Li/LFP half-cell

Symbol	Unit	Range		Estimated value
		min	max	
$D_{s,p}$	m^2/s	1.0e-19	1.0e-17	8.25e-18
K_p	m$^{2.5}$/mol$^{0.5}$ s	5.0e-13	5e-12	1.826e-12
ε_p	-	0.15	0.30	0.263
a_1	Ωm^2	2e-4	2e-3	6.3539e-4
a_2	-	1	10	3.819
a_3	Ωm^2	2e-3	6e-3	4.8e-3

Figure 4.4 and Figure 4.5 illustrate good agreements between simulated and experimental potential in discharge and charge process, respectively. Here, even in moderate C-rate, SPM coupled with the use of an exponential resistance shows promising results.

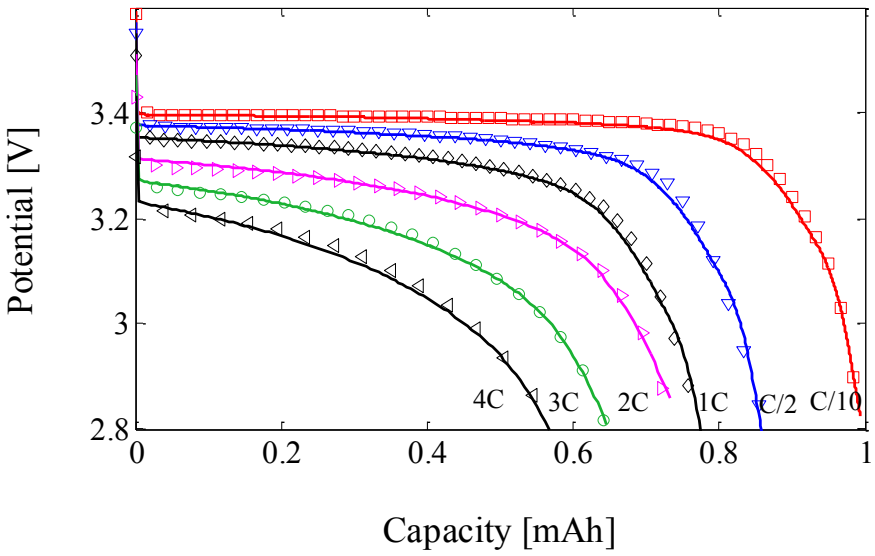

Figure 4.4: Simulated (solid lines) and experimental (symbols) discharge curves for high-power cell

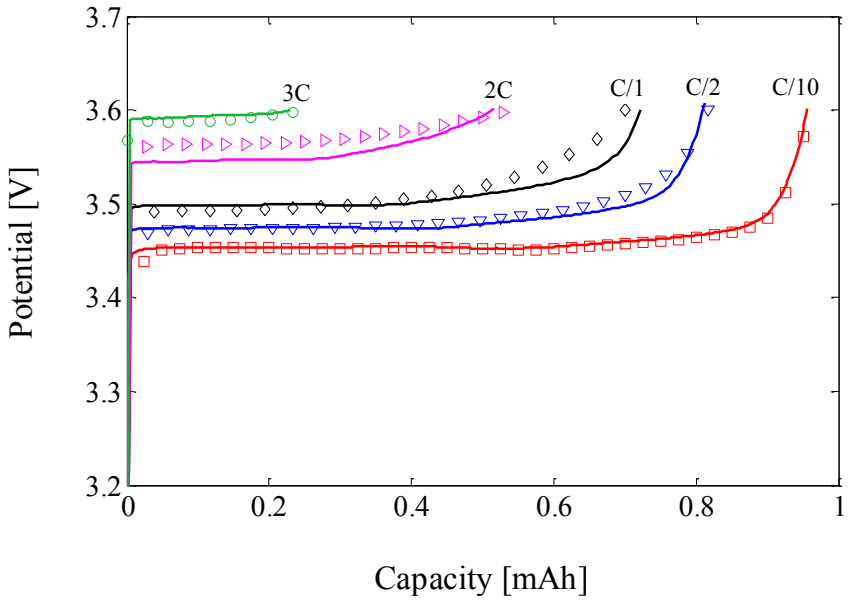

Figure 4.5: Simulated (solid lines) and experimental (symbols) charge curves for high-power cell

In parameter estimation studies, it is important to check the risk of over-fitting. Over-fitting in PE studies happens when the number of parameters is large and the inverse method finds the parameters that are more representative of the noise of the system than representing the general trend. Although the estimated parameters simulate the performance perfectly, they are inefficient to study the behavior of the cell in other conditions. One way to examine the over-fitting is to test the model in a new condition that differs from conditions that are used for PE.

In this regard, the model is verified by simulating potential for a discharge rate of 4C (also depicted in Figure 4.4). Here, the estimated parameters are based on lower discharge rates (mentioned in Table 4.2). Obviously, the predictability of the model is good enough outside the conditions used for PE.

The estimated particle radius for both charge and discharge process is depicted in Figure 4.6. It is seen that the higher the discharge current is, the smaller gets the particle radius, which is in agreement with the Mosaic model.

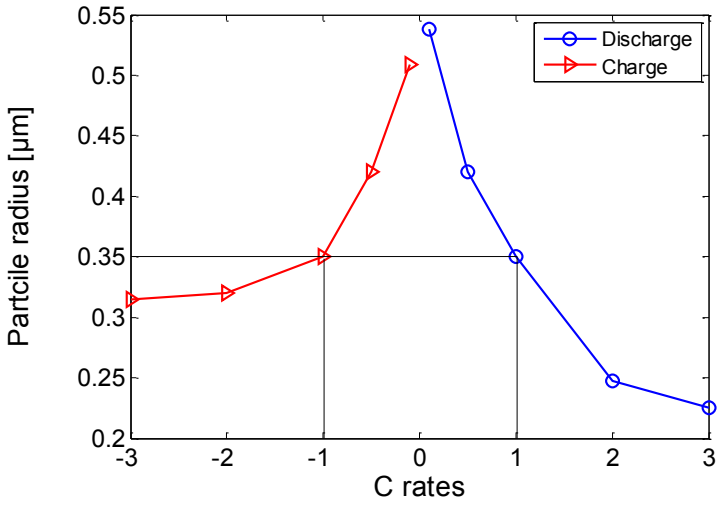

Figure 4.6: Apparent particle radius in each charge/discharge current from the PE and the SPM

A changing load test was performed to verify efficiency of the model. In this regard, a fully charge cell is discharged with 3C rate for 8 minutes. This follows by a charge and discharge process each with 2C rate in 8 minutes. Finally, 15 minutes of charge and 15 minutes of discharge are applied with 1C rate. Figure 4.7 demonstrates the experimental data and simulated results where a good agreement is evident.

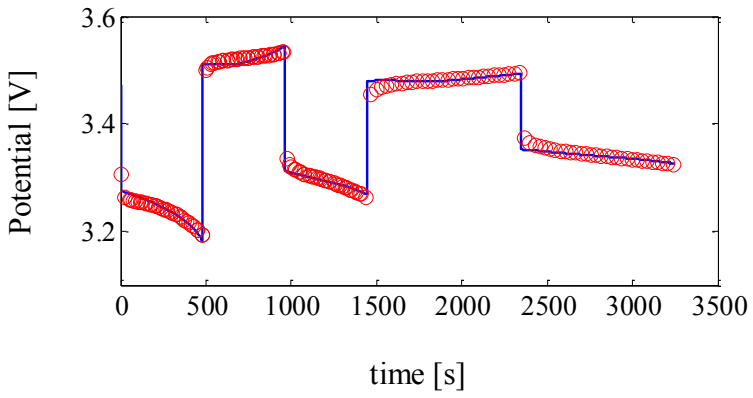

Figure 4.7: Simulated (solid lines) and experimental (symbols) potential of high-power Li/LFP half-cell for a variable load

It is generally easier to model cells designed for high-power applications because, in this case, the electrodes are thinner and the overpotentials are smaller. However, it is necessary to check the accuracy of the model for cells with different applications. Therefore, the validity of the model is examined here for thicker positive electrode in order to justify its capability. Figure 4.8 illustrates the comparison between the model estimations and the experimental measurements for high-energy Li/LFP cell.

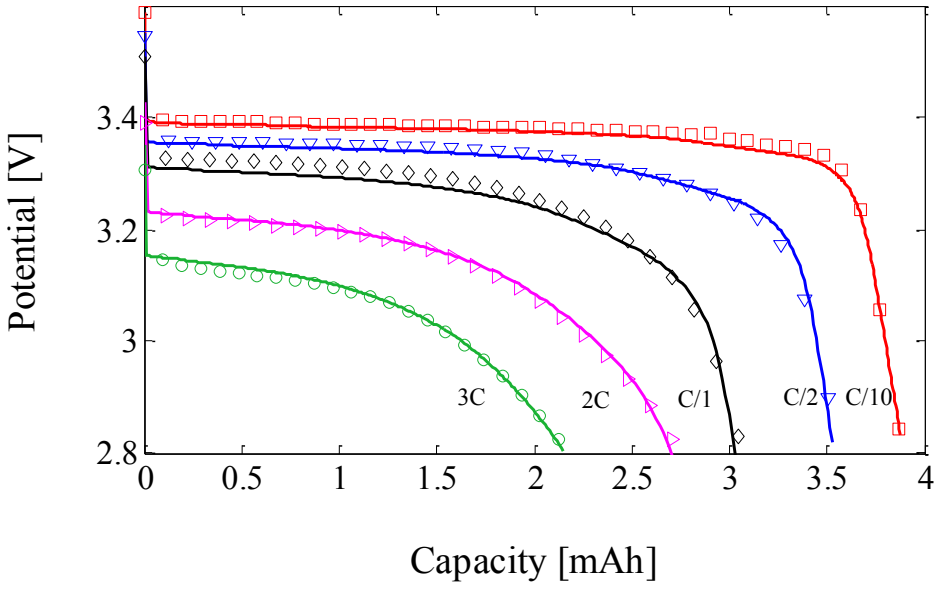

Figure 4.8: Simulated (solid line) and experimental (symbols) discharge curves for high-energy cell

As seen in Figure 4.8, a good agreement is achieved between the simulation results and the experimental measurements, this time with the thicker positive electrode design. The estimated parameters for such a configuration, which are the porosity of the electrode (ε_p), the unknown coefficients in the cell resistance equation (a_1, a_2 and a_3 in Eq. (4.14)) and the radius of particles in each discharge current (except 1C), are provided in Table 4.3. The solid diffusion coefficient ($D_{s,p}$), and the intercalation/deintercalation reaction-rate constant (K_p) are chosen to be the same as in case of the high-power cell design.

Table 4.3: Estimated parameters for the high-energy Li/LFP half-cell

Symbol	Unit	Range		Estimated value
		min	max	
ε_p	-	0.15	0.30	0.263
a_1	Ωm^2	6e-6	8e-5	3.7891e-05
a_2	-	2	20	6.2385
a_3	Ωm^2	2e-3	6e-3	3.9e-3

Using Eq. (4.15), the specific error values for each discharge curve is calculated for both high-energy and high-power Li cells. The values for specific error are summarized in Table 4.4.

$$e_s = \left(\frac{1}{N}\right)\sum_{i=1}^{N}\left(V^*_{cell,m,i} - V_{cell,i}(\mathbf{P})\right)^2 \tag{4.15}$$

Table 4.4: Specific error values of all discharge curves for each cathode material

e_s	C/10	C/2	1C	2C	3C	4C
High power	9.25×10^{-5}	1.35×10^{-4}	1.24×10^{-4}	9.28×10^{-5}	1.23×10^{-4}	2.69×10^{-4}
High energy	1.27×10^{-4}	1.42×10^{-4}	3.59×10^{-4}	7.92×10^{-5}	1.57×10^{-4}	-

Although the errors are very low and acceptable, it seems that no correlation exists between the errors and the discharge rates. In another word, the error does not increase while higher discharge rates are simulated. An interpretation can be that for higher discharge rates, the resistance of cell behaves closer to the exponential form of the equation (Eq. (4.14), which compensates the higher error of SPM simulation in high discharge rates.

4.6 Conclusion

An empirical variable resistance has been added inside a Single Particle Model (SPM) to represent the increasing overpotential specifically found at the end of the charge/discharge process of a Li/LFP cell. This improved SPM model takes into account 1- the increasing diffusion overpotential due to the intercalation/deintercalation of ions in larger particles and 2- the increasing ohmic resistance from the resistive-reactant feature of LFP. The electrolyte overpotential can also be a part of this increasing resistance, which makes the model well suited for charge/discharge rates higher than 1C. Parameter Estimation method provided the electrochemical parameters of the cell and the constant coefficients of the empirical function of resistance. A current-dependent radius (Mosaic model) was considered for the particles to mimic the particle-size distribution (PSD). Model-experiment comparisons indicated promising results for two designs of Li/LFP coin cells, a high-power and a high-capacity configurations.

Acknowledgements

The authors are very grateful to Hydro-Québec and to the Natural Sciences and Engineering Council of Canada (NSERC) for their financial support.

Nomenclature:

$c_{s,k}^{\max}$	Maximum concentration of Li^+ in the particle of positive electrode, mol/m^3
$D_{s,p}$	Li^+ diffusion coefficient in the particle of positive electrode, m^2/s
F	Faraday's constant, C/mol
I	Applied current density, A/m^2
K_k	Reaction rate constant of electrode *k (k=p,n)*, $m^{2.5}/mol^{0.5}s$
$\mathbf{P}$	Unknown parameter vector
R	Universal gas constant, J/mol K
R_p	Radius of the particles of positive electrode, m

S_k	Total electroactive area of electrode *k (k=p,n)*, m^2
SOC_p	State of charge of positive electrode
$SOC_{p,ini}$	Initial state of charge of positive electrode
t	Time, s
T	Absolute temperature, K
U_p	Open-circuit potential of positive electrode, V
V_p	Total volume of positive, m^3
$\mathbf{v}_{cell}$	Model's estimation of the cell potential, V

Greek

ε_p	Porosity of positive electrode
δ_p	Dimensionless flux of lithium ion at positive electrode
λ_k	The *k*th eigenvalue

Subscripts

ini	Initial state
p	Positive electrode
n	Negative electrode
s	Solid phase

5. Conclusion

The research project presented in this thesis is divided in two parts: 1. developing a PE methodology to estimate the main electrochemical parameters of LIBs, and 2. introducing a simple model to simulate the peculiar behavior of LIB with LFP as the positive electrode material. The proposed PE methodology showed promising results for simulating LIBs with three different positive electrode active materials including $LiCoO_2$, $LiMn_2O_4$ and $LiFePO_4$, thus expressing its full potential and flexibility. As the second main objective, PE have been successfully used to calculate the most influential electrochemical parameters of LFP positive electrode and the coefficients of the newly proposed variable resistance SPM. Again, a good agreement has been found when experimental data were compared to the model predictions.

A well-suited model for the simulation of LIBs depends on the desired time and length scales. Increasing demands for employing LIBs in electric and hybrid electric vehicles (EV/HEV) in the form of a battery pack integrated to an efficient battery management system (BMS) necessitate selecting an appropriate model for large time and length scales. Considering kinetics and mass transport inside the cell, electrochemical engineering models surpass other models available in the open literature. Although SPM neglects the concentration and potential fields in the solution phase, it still appears to be the best candidate among other electrochemical models for PE and large time/length scale studies. Here, a modified SPM is derived from a P2D model assuming a linear function for the electrolyte concentration and a polynomial function for its conductivity. This modification succeeds to enhance SPM with an electrolyte potential drop function and makes it more accurate in higher discharge/charge rate simulations. PE provides parameters that SPM needs. These parameters include design parameters, electrode specific parameters and kinetics parameters. In the work presented, eight key internal parameters of LIB determined by PE have been identified: the solid diffusion coefficients ($D_{s,n}$ and $D_{s,p}$), the intercalation/deintercalation reaction-rate constants (K_n and K_p), the initial SOC ($SOC_{n,0}$ and $SOC_{p,0}$), and the electroactive surface areas (S_n and S_p). In this study, PE is also used to determine the two coefficients of the newly introduced electrolyte potential drop function. A sensitivity analysis is conducted for defining the best time domains to estimate each parameter. Although these parameters are identifiable with the Li-ion direct model, their magnitude is dependent on the positive and negative materials. Moreover, various structures of the active materials and different intercalation/deintercalation mechanisms call for the application of the methodology for each different positive electrode active materials. Accordingly, separated sensitivity analyses were carried out for each material.

After achieving good results with the PE methodology presented in chapter three, special features of LFP active material were addressed and a variable resistance SPM was introduced to represent these characteristics. Again, major parameters of LFP electrode were estimated. In

addition, three coefficients of an exponential equation representing the resistivity of LFP were determined to illustrate the increasing overpotential drop at the end of the discharge process. This resistive behavior of LFP was attributed to two phenomena: 1. increasing diffusion overpotential from intercalation / deintercalation of ions in larger particles at the end of discharge, and 2. higher ohmic resistance due to transfer of electrons inside low conductive matrix phase as the discharge proceeds. The varying resistance SPM displayed improvements in modeling the behavior of LFP electrode in both case of high-energy and high-power Li/LFP coin cells.

5.1 Future work

The systematic and accurate PE methodology presented in this study is the first step toward a better estimation of the inside electrochemical parameters of LIBs. Although the methodology and the process were verified for different electrode active materials, it is always necessary to check the predictability of the methodology when it comes to estimate parameters of new materials with a different structure. Moreover, it would be of merit to expand this study by modifying the assumptions in the direct electrochemical model. However, it should be noted that enhancing the model could jeopardize the speed of the PE process and make the methodology inconvenient for the online estimation. For example, adding temperature equations and heat generation relationships would improve the predictability of PE in various working temperature. In this case, the needed calculation time, however, will increase due to coupling of electrochemical equation and thermal ones.

One of the best scenario for pursuing this study is to perform PE during lifetime of the cells in different time intervals and cycle numbers. Due to the fact that electrochemical parameters are representing the physical phenomena occurring inside the cells, following the changes in these parameters will shed light on the mechanisms and phenomena taking place when the battery ages. In this regard, attributing appropriate empirical functions for each dominant parameter will lead to the development of a semi-empirical aging model.

References

[1] Dunn, B., Kamath, H., & Tarascon, J. M. (2011). Electrical energy storage for the grid: a battery of choices. *Science*, *334*(6058), 928-935.

[2] Tarascon, J. M., & Armand, M. (2001). Issues and challenges facing rechargeable lithium batteries. *Nature*, *414*(6861), 359-367.

[3] Park, J. K. (Ed.). (2012). *Principles and applications of lithium secondary batteries*. John Wiley & Sons.

[4] Bloom, I., Cole, B. W., Sohn, J. J., Jones, S. A., Polzin, E. G., Battaglia, V. S., ... & Ingersoll, D. (2001). An accelerated calendar and cycle life study of Li-ion cells. *Journal of Power Sources*, *101*(2), 238-247.

[5] Liaw, B. Y., Jungst, R. G., Nagasubramanian, G., Case, H. L., & Doughty, D. H. (2005). Modeling capacity fade in lithium-ion cells. *Journal of power sources*, *140*(1), 157-161.

[6] Atlung, S., West, K., & Jacobsen, T. (1979). Dynamic aspects of solid solution cathodes for electrochemical power sources. *Journal of The Electrochemical Society*, *126*(8), 1311-1321.

[7] Haran, B. S., Popov, B. N., & White, R. E. (1998). Determination of the hydrogen diffusion coefficient in metal hydrides by impedance spectroscopy. *Journal of Power Sources*, *75*(1), 56-63.

[8] Guo, M., Sikha, G., & White, R. E. (2011). Single-particle model for a lithium-ion cell: Thermal behavior. *Journal of The Electrochemical Society*, *158*(2), A122-A132.

[9] Zhang, D., Popov, B. N., & White, R. E. (2000). Modeling lithium intercalation of a single spinel particle under potentiodynamic control. *Journal of The Electrochemical Society*, *147*(3), 831-838.

[10] Santhanagopalan, S., Guo, Q., Ramadass, P., & White, R. E. (2006). Review of models for predicting the cycling performance of lithium ion batteries. *Journal of Power Sources*, *156*(2), 620-628.

[11] Ramadesigan, V., Northrop, P. W., De, S., Santhanagopalan, S., Braatz, R. D., & Subramanian, V. R. (2012). Modeling and simulation of lithium-ion batteries from a systems engineering perspective. *Journal of The Electrochemical Society*, *159*(3), R31-R45.

[12] Doyle, M., & Newman, J. (1995). Modeling the performance of rechargeable lithium-based cells: design correlations for limiting cases. *Journal of Power Sources*, *54*(1), 46-51.

[13] Doyle, M., & Newman, J. (1995). The use of mathematical modeling in the design of lithium/polymer battery systems. *Electrochimica Acta*, *40*(13), 2191-2196.

[14] Newman, J. (1995). Optimization of Porosity and Thickness of a Battery Electrode by Means of a Reaction-Zone Model. *Journal of the Electrochemical Society*, *142*(1), 97-101.

[15] Botte, G. G., Subramanian, V. R., & White, R. E. (2000). Mathematical modeling of secondary lithium batteries. *Electrochimica Acta*, *45*(15), 2595-2609.

[16] Doyle, M., Newman, J., Gozdz, A. S., Schmutz, C. N., & Tarascon, J. M. (1996). Comparison of modeling predictions with experimental data from plastic lithium ion cells. *Journal of the Electrochemical Society*, *143*(6), 1890-1903.

[17] Fuller, T. F., Doyle, M., & Newman, J. (1994). Relaxation Phenomena in Lithium-Ion-Insertion Cells. *Journal of the Electrochemical Society*, *141*(4), 982-990.

[18] Fuller, T. F., Doyle, M., & Newman, J. (1994). Simulation and optimization of the dual lithium ion insertion cell. *Journal of the Electrochemical Society*, *141*(1), 1-10.

[19] Gomadam, P. M., Weidner, J. W., Dougal, R. A., & White, R. E. (2002). Mathematical modeling of lithium-ion and nickel battery systems. *Journal of Power Sources*, *110*(2), 267-284.

[20] Ning, G., White, R. E., & Popov, B. N. (2006). A generalized cycle life model of rechargeable Li-ion batteries. *Electrochimica acta*, *51*(10), 2012-2022.

[21] Ramadass, P., Haran, B., Gomadam, P. M., White, R., & Popov, B. N. (2004). Development of first principles capacity fade model for Li-ion cells. *Journal of the Electrochemical Society*, *151*(2), A196-A203.

[22] Thomas, K. E., & Newman, J. (2003). Thermal modeling of porous insertion electrodes. *Journal of the Electrochemical Society*, *150*(2), A176-A192.

[23] Bhattacharya, J., & Van der Ven, A. (2010). Phase stability and nondilute Li diffusion in spinel Li 1+ x Ti 2 O 4. *Physical Review B*, *81*(10), 104304.

[24] Van der Ven, A., Bhattacharya, J., & Belak, A. A. (2012). Understanding Li diffusion in Li-intercalation compounds. *Accounts of chemical research*, *46*(5), 1216-1225.

[25] Ceder, G., Abdellahi, A., Akyildiz, O., Malik, R., & Thornton, K. (2013, October). Phase transformation kinetics and morphology in LiFePO4. In *Meeting Abstracts* (No. 11, pp. 575-575). The Electrochemical Society.

[26] Newman, J., & Tiedemann, W. (1975). Porous-electrode theory with battery applications. *AIChE Journal*, *21*(1), 25-41.

[27] Bruggeman, D. A. G. (1935). Calculation of various physics constants in heterogenous substances I Dielectricity constants and conductivity of mixed bodies from isotropic substances. *Ann. Phys*, *24*(7), 636-664.

[28] Thomas, K. E., Newman, J., & Darling, R. M. (2002). Mathematical modeling of lithium batteries. In *Advances in lithium-ion batteries* (pp. 345-392). Springer US.

[29] Safari, M., Morcrette, M., Teyssot, A., & Delacourt, C. (2009). Multimodal physics-based aging model for life prediction of Li-ion batteries. *Journal of The Electrochemical Society*, *156*(3), A145-A153.

[30] Ning, G., & Popov, B. N. (2004). Cycle life modeling of lithium-ion batteries. *Journal of The Electrochemical Society*, *151*(10), A1584-A1591.

[31] Safari, M., & Delacourt, C. (2011). Mathematical modeling of lithium iron phosphate electrode: galvanostatic charge/discharge and path dependence. *Journal of The Electrochemical Society*, *158*(2), A63-A73.

[32] Tanim, T. R., Rahn, C. D., & Wang, C. Y. (2015). A temperature dependent, single particle, lithium ion cell model including electrolyte diffusion. *Journal of Dynamic Systems, Measurement, and Control*, *137*(1), 011005.

[33] Rahimian, S. K., Rayman, S., & White, R. E. (2013). Extension of physics-based single particle model for higher charge–discharge rates. *Journal of Power Sources*, *224*, 180-194.

[34] Santhanagopalan, S., Guo, Q., & White, R. E. (2007). Parameter estimation and model discrimination for a lithium-ion cell. *Journal of the Electrochemical Society*, *154*(3), A198-A206.

[35] Santhanagopalan, S., Zhang, Q., Kumaresan, K., & White, R. E. (2008). Parameter estimation and life modeling of lithium-ion cells. *Journal of The Electrochemical Society*, *155*(4), A345-A353.

[36] Ramadesigan, V., Chen, K., Burns, N. A., Boovaragavan, V., Braatz, R. D., & Subramanian, V. R. (2011). Parameter estimation and capacity fade analysis of lithium-ion batteries using reformulated models. *Journal of The Electrochemical Society*, *158*(9), A1048-A1054.

[37] Marcicki, J., Canova, M., Conlisk, A. T., & Rizzoni, G. (2013). Design and parametrization analysis of a reduced-order electrochemical model of graphite/LiFePO 4 cells for SOC/SOH estimation. *Journal of Power Sources*, *237*, 310-324.

[38] Zhang, L., Wang, L., Hinds, G., Lyu, C., Zheng, J., & Li, J. (2014). Multi-objective optimization of lithium-ion battery model using genetic algorithm approach. *Journal of Power Sources*, *270*, 367-378.

[39] Forman, J. C., Moura, S. J., Stein, J. L., & Fathy, H. K. (2012). Genetic identification and fisher identifiability analysis of the Doyle–Fuller–Newman model from experimental cycling of a LiFePO4 cell. *Journal of Power Sources*, *210*, 263-275.

[40] Jokar, A., Rajabloo, B., Désilets, M., & Lacroix, M. (2016). An Inverse Method for Estimating the Electrochemical Parameters of Lithium-Ion Batteries I. Methodology. *Journal of The Electrochemical Society*, *163*(14), A2876-A2886.

[41] Masoudi, R., Uchida, T., & McPhee, J. (2015). Parameter estimation of an electrochemistry-based lithium-ion battery model. *Journal of Power Sources*, *291*, 215-224.

[42] Rahman, M. A., Anwar, S., & Izadian, A. (2016). Electrochemical model parameter identification of a lithium-ion battery using particle swarm optimization method. *Journal of Power Sources*, *307*, 86-97.

[43] Ozisik, M. N. (2000). *Inverse heat transfer: fundamentals and applications*. CRC Press.

[44] Colaço, M. J., Orlande, H. R., & Dulikravich, G. S. (2006). Inverse and optimization problems in heat transfer. *Journal of the Brazilian Society of Mechanical Sciences and Engineering*, *28*(1), 1-24.

[45] Rajabloo, B., Jokar, A., Désilets, M., & Lacroix, M. (2017). An Inverse Method for Estimating the Electrochemical Parameters of Lithium-Ion Batteries II: Implementation. *Journal of The Electrochemical Society*, *164*(2), A99-A105.

[46] Zhang, J., & Lee, J. (2011). A review on prognostics and health monitoring of Li-ion battery. *Journal of Power Sources*, *196*(15), 6007-6014.

[47] Lu, L., Han, X., Li, J., Hua, J., & Ouyang, M. (2013). A review on the key issues for lithium-ion battery management in electric vehicles. *Journal of power sources*, *226*, 272-288.

[48] Rahimi-Eichi, H., Ojha, U., Baronti, F., & Chow, M. Y. (2013). Battery management system: an overview of its application in the smart grid and electric vehicles. *IEEE Industrial Electronics Magazine*, *7*(2), 4-16.

[49] Doyle, M., Fuller, T. F., & Newman, J. (1993). Modeling of galvanostatic charge and discharge of the lithium/polymer/insertion cell. *Journal of the Electrochemical Society*, *140*(6), 1526-1533.

[50] Jokar, A., Rajabloo, B., Désilets, M., & Lacroix, M. (2016). Review of simplified Pseudo-two-Dimensional models of lithium-ion batteries. *Journal of Power Sources*, *327*, 44-55.

[51] Masoudi, R., Uchida, T., & McPhee, J. (2015). Parameter estimation of an electrochemistry-based lithium-ion battery model. *Journal of Power Sources*, *291*, 215-224.

[52] Seaman, A., Dao, T. S., & McPhee, J. (2014). A survey of mathematics-based equivalent-circuit and electrochemical battery models for hybrid and electric vehicle simulation. *Journal of Power Sources*, *256*, 410-423.

[53] Cai, L., & White, R. E. (2009). Reduction of model order based on proper orthogonal decomposition for lithium-ion battery simulations. *Journal of The Electrochemical Society*, *156*(3), A154-A161.

[54] Prosini, P. P., Lisi, M., Scaccia, S., Carewska, M., Cardellini, F., & Pasquali, M. (2002). Synthesis and characterization of amorphous hydrated FePO4 and its electrode performance in lithium batteries. *Journal of the Electrochemical Society*, *149*(3), A297-A301.

[55] Prosini, P. P., Lisi, M., Zane, D., & Pasquali, M. (2002). Determination of the chemical diffusion coefficient of lithium in LiFePO 4. *Solid State Ionics*, *148*(1), 45-51.

[56] Denis, Y. W., Fietzek, C., Weydanz, W., Donoue, K., Inoue, T., Kurokawa, H., & Fujitani, S. (2007). Study of LiFePO4 by cyclic voltammetry. *Journal of the Electrochemical Society*, *154*(4), A253-A257.

[57] Churikov, A. V., Ivanishchev, A. V., Ivanishcheva, I. A., Sycheva, V. O., Khasanova, N. R., & Antipov, E. V. (2010). Determination of lithium diffusion coefficient in LiFePO 4 electrode by galvanostatic and potentiostatic intermittent titration techniques. *Electrochimica Acta*, *55*(8), 2939-2950.

[58] Matsui, H., Nakamura, T., Kobayashi, Y., Tabuchi, M., & Yamada, Y. (2010). Open-circuit voltage study on LiFePO 4 olivine cathode. *Journal of Power Sources*, *195*(19), 6879-6883.

[59] Tang, X. C., Li, L. X., Lai, Q. L., Song, X. W., & Jiang, L. H. (2009). Investigation on diffusion behavior of Li+ in LiFePO 4 by capacity intermittent titration technique (CITT). *Electrochimica Acta*, *54*(8), 2329-2334.

[60] Srinivasan, V., & Newman, J. (2004). Design and optimization of a natural graphite/iron phosphate lithium-ion cell. *Journal of the Electrochemical Society*, *151*(10), A1530-A1538.

[61] Yu, S., Kim, S., Kim, T. Y., Nam, J. H., & Cho, W. I. (2013). Model Prediction and Experiments for the Electrode Design Optimization of LiFePO4/Graphite Electrodes in High Capacity Lithium-ion Batteries. *Bull. Korean Chem. Soc*, *34*(1), 79.

[62] Prada, E., Di Domenico, D., Creff, Y., Bernard, J., Sauvant-Moynot, V., & Huet, F. (2012). Simplified electrochemical and thermal model of LiFePO4-graphite Li-ion batteries for fast charge applications. *Journal of The Electrochemical Society*, *159*(9), A1508-A1519.

[63] Safari, M., & Delacourt, C. (2011). Modeling of a commercial graphite/LiFePO4 cell. *Journal of The Electrochemical Society*, *158*(5), A562-A571.

[64] Doyle, M., & Fuentes, Y. (2003). Computer simulations of a lithium-ion polymer battery and implications for higher capacity next-generation battery designs. *Journal of The Electrochemical Society*, *150*(6), A706-A713.

[65] Maheshwari, A., Dumitrescu, M. A., Destro, M., & Santarelli, M. (2016). Inverse parameter determination in the development of an optimized lithium iron phosphate–Graphite battery discharge model. *Journal of Power Sources*, *307*, 160-172.

[66] Srinivasan, V., & Newman, J. (2004). Discharge model for the lithium iron-phosphate electrode. *Journal of the Electrochemical Society*, *151*(10), A1517-A1529.

[67] Dodd, J. L. (2007). *Phase composition and dynamical studies of lithium iron phosphate* (Doctoral dissertation, California Institute of Technology).

[68] Li, J., Cheng, Y., Jia, M., Tang, Y., Lin, Y., Zhang, Z., & Liu, Y. (2014). An electrochemical–thermal model based on dynamic responses for lithium iron phosphate battery. *Journal of Power Sources*, *255*, 130-143.

[69] Kumaresan, K., Sikha, G., & White, R. E. (2008). Thermal model for a Li-ion cell. *Journal of the Electrochemical Society*, *155*(2), A164-A171.

[70] Farkhondeh, M., Safari, M., Pritzker, M., Fowler, M., Han, T., Wang, J., & Delacourt, C. (2014). Full-range simulation of a commercial LiFePO4 electrode accounting for bulk and surface effects: A comparative analysis. *Journal of The Electrochemical Society*, *161*(3), A201-A212.

[71] Andersson, A. S., & Thomas, J. O. (2001). The source of first-cycle capacity loss in LiFePO 4. *Journal of Power Sources*, *97*, 498-502.

[72] Ravet, N., Goodenough, J. B., Besner, S., Simoneau, M., Hovington, P., & Armand, M. (1999, October). Abstract# 127, 196. In *Meeting of the Electrochemical Society, Hawai*.

[73] Ravet, N., Chouinard, Y., Magnan, J. F., Besner, S., Gauthier, M., & Armand, M. (2001). Electroactivity of natural and synthetic triphylite. *Journal of Power Sources*, *97*, 503-507.

[74] Yamada, A., Chung, S. C., & Hinokuma, K. (2001). Optimized LiFePO4 for lithium battery cathodes. *Journal of the electrochemical society*, *148*(3), A224-A229.

[75] Delacourt, C., Poizot, P., Levasseur, S., & Masquelier, C. (2006). Size effects on carbon-free LiFePO4 powders the key to superior energy density. *Electrochemical and Solid-State Letters*, *9*(7), A352-A355.

[76] Huang, H., Yin, S. C., & Nazar, L. S. (2001). Approaching theoretical capacity of LiFePO4 at room temperature at high rates. *Electrochemical and Solid-State Letters*, *4*(10), A170-A172.

[77] Laffont, L., Delacourt, C., Gibot, P., Wu, M. Y., Kooyman, P., Masquelier, C., & Tarascon, J. M. (2006). Study of the LiFePO4/FePO4 two-phase system by high-resolution electron energy loss spectroscopy. *Chemistry of Materials*, *18*(23), 5520-5529.

[78] Bramnik, N. N., Nikolowski, K., Baehtz, C., Bramnik, K. G., & Ehrenberg, H. (2007). Phase transitions occurring upon lithium insertion-extraction of LiCoPO4. *Chemistry of Materials*, *19*(4), 908-915.

[79] Padhi, A. _. K., Nanjundaswamy, K. S., & Goodenough, J. B. D. (1997). Phospho-olivines as positive-electrode materials for rechargeable lithium batteries. *Journal of the electrochemical society*, *144*(4), 1188-1194.

[80] Yamada, A., Koizumi, H., Sonoyama, N., & Kanno, R. (2005). Phase change in Li x FePO4. *Electrochemical and Solid-State Letters*, *8*(8), A409-A413.

[81] Kasavajjula, U. S., Wang, C., & Arce, P. E. (2008). Discharge model for LiFePO4 accounting for the solid solution range. *Journal of The Electrochemical Society*, *155*(11), A866-A874.

[82] Dargaville, S., & Farrell, T. W. (2010). Predicting active material utilization in LiFePO4 electrodes using a multiscale mathematical model. *Journal of the Electrochemical Society*, *157*(7), A830-A840.

[83] Singh, G. K., Ceder, G., & Bazant, M. Z. (2008). Intercalation dynamics in rechargeable battery materials: general theory and phase-transformation waves in LiFePO 4. *Electrochimica Acta*, *53*(26), 7599-7613.

[84] Burch, D., Singh, G., Ceder, G., & Bazant, M. Z. (2008). Phase-transformation wave dynamics in LiFePO4. In *Solid State Phenomena* (Vol. 139, pp. 95-100). Trans Tech Publications.

[85] Burch, D., & Bazant, M. Z. (2009). Size-dependent spinodal and miscibility gaps for intercalation in nanoparticles. *Nano letters*, *9*(11), 3795-3800.

[86] Delmas, C., Maccario, M., Croguennec, L., Le Cras, F., & Weill, F. (2008). Lithium deintercalation in LiFePO4 nanoparticles via a domino-cascade model. *Nature materials*, *7*(8), 665-671.

[87] Sasaki, T., Ukyo, Y., & Novák, P. (2013). Memory effect in a lithium-ion battery. *Nature materials*, *12*(6), 569-575.

[88] Thomas-Alyea, K. E. (2008). Modeling resistive-reactant and phase-change materials in battery electrodes. *ECS Transactions*, *16*(13), 155-165.

[89] Thorat, I. V. (2009). *Understanding Performance-limiting Mechanisms in Lithium-ion Batteries for High-rate Applications*. ProQuest.

[90] Farkhondeh, M., & Delacourt, C. (2011). Mathematical modeling of commercial LiFePO4 electrodes based on variable solid-state diffusivity. *Journal of The Electrochemical Society*, *159*(2), A177-A192.

[91] Wang, J., & Sun, X. (2015). Olivine LiFePO 4: the remaining challenges for future energy storage. *Energy & Environmental Science*, *8*(4), 1110-1138.

[92] Delacourt, C., & Safari, M. (2011). Analysis of lithium deinsertion/insertion in Li y FePO 4 with a simple mathematical model. *Electrochimica Acta*, *56*(14), 5222-5229.

[93] Delacourt, C., Laffont, L., Bouchet, R., Wurm, C., Leriche, J. B., Morcrette, M. & Masquelier, C. (2005). Toward understanding of electrical limitations (electronic, ionic) in LiMPO4 (M= Fe, Mn) electrode materials. *Journal of the Electrochemical Society*, *152*(5), A913-A921.

[94] Dominko, R., Gaberscek, M., Drofenik, J., Bele, M., Pejovnik, S., & Jamnik, J. (2003). The role of carbon black distribution in cathodes for Li ion batteries. *Journal of Power Sources*, *119*, 770-773.

[95] Marcicki, J. (2012). *Modeling, parametrization, and diagnostics for lithium-ion batteries with automotive applications* (Doctoral dissertation, The Ohio State University).

[96] Arora, P., Doyle, M., Gozdz, A. S., White, R. E., & Newman, J. (2000). Comparison between computer simulations and experimental data for high-rate discharges of plastic lithium-ion batteries. *Journal of power Sources*, *88*(2), 219-231.

[97] Paxton, B., & Newman, J. (1996). Variable Diffusivity in Intercalation Materials A Theoretical Approach. *Journal of The Electrochemical Society*, *143*(4), 1287-1292.

[98] Franger, S. F. L. C., Le Cras, F., Bourbon, C., & Rouault, H. (2002). LiFePO4 synthesis routes for enhanced electrochemical performance. *Electrochemical and Solid-State Letters*, *5*(10), A231-A233.